Sedimentary Geology 290 (2013) 109–125

Contents lists available at SciVerse ScienceDirect

Sedimentary Geology

journal homepage: www.elsevier.com/locate/sedgeo

Provenance of Tertiary sandstone in the northern Qaidam basin, northeastern Tibetan Plateau: Integration of framework petrography, heavy mineral analysis and mineral chemistry

Xing Jian [a], Ping Guan [a,*], Dao-Wei Zhang [b], Wei Zhang [a,c], Fan Feng [a], Rui-Juan Liu [a], Si-Da Lin [a]

[a] Ministry of Education Key Laboratory of Orogenic Belts and Crustal Evolution, School of Earth and Space Sciences, Peking University, Beijing 100871, PR China
[b] Qinghai Oilfield Company, PetroChina, Dunhuang 736202, PR China
[c] Research Institute of Petroleum Exploration & Development, PetroChina, Beijing 100083, PR China

ARTICLE INFO

Article history:
Received 24 February 2012
Received in revised form 6 March 2013
Accepted 9 March 2013
Available online 16 March 2013

Dr. B. Jones

Keywords:
Tibetan Plateau
Qaidam basin
Tertiary
Provenance
Heavy mineral analysis
Log-ratio confidence region

ABSTRACT

An exceptionally thick Cenozoic sedimentary succession has developed in the Qaidam basin of the northeastern Tibetan Plateau. The provenance remains enigmatic; thus, more precise investigations are needed. An integrated study of sandstone framework petrography, heavy mineral analysis and mineral chemistry was adopted to perform provenance analysis of the Tertiary sandstones in the northern Qaidam basin.

No individual method exists that can provide comprehensive provenance interpretations on spatial and temporal variations. Based on three types of data, three depositional areas can be distinguished. Sandstones of Area A exhibit relatively high abundances of quartz, garnet and zircon, as well as relatively high textural maturity, implying long-distance sources. Multi-composition garnets and tourmalines reveal derivations of metasedimentary rocks and intermediate-acidic igneous rocks. Sandstones of Area B are rich in metamorphic lithic fragments, epidote and garnet. A dominance of Fe-rich garnets with low Mg, low Mn and variable Ca contents and dravites demonstrates predominant derivation of metasedimentary rocks. Therefore, the North Qaidam and South Qilian terranes are potential source areas for these two depositional areas. Additionally, high metamorphic heavy mineral abundances in the upper formations imply increasing contributions of these two metamorphic belts during the Tertiary tectonic uplift. However, sandstones of Area C are characterized by relatively high abundances of feldspar, igneous heavy minerals and high-Fe + Mn garnet, which suggest a main source of igneous rocks. The Altun and Qilian Mountains are potential source regions. Furthermore, increasing amounts of feldspar and igneous heavy minerals in the upper formations indicate a significant presence of igneous parent rocks, which are most likely a response to the multi-stage uplift events in the Altun Mountains since the early Eocene.

1. Introduction

The Qaidam basin is the largest continental basin in the northeastern Tibetan Plateau. It contains an exceptionally thick Tertiary sedimentary succession, with an average thickness up to 6 km (Hanson et al., 2001). This thick and continuous sedimentary record preserves substantial information about the tectonic settings of provenance and source rock lithology, as well as the tectonic evolution of the northeastern Tibetan Plateau. All clastic materials in the Qaidam basin are derived from source areas via drainage systems. Due to the immense volume of Tertiary sediments (Wang et al., 2006), it must be considered whether the source rocks experienced significant spatial and temporal changes. Moreover, the sediment provenance interpretation of the Qaidam basin can also provide helpful data regarding the tectonic uplift, exhumation and unroofing history of orogens in the northeastern Tibetan Plateau.

Previous studies primarily focused on the surrounding mountains and emphasized the mineralogy, petrology and geochronology of the current source rocks of the basin (e.g., Mattinson et al., 2007; Song et al., 2007a,b; Zhang et al., 2008a). Some studies discussed the tectonic history and climatic evolution of the Qaidam basin (e.g., Liu et al., 1998; Wang et al., 1999; Yin et al., 2002; Rieser et al., 2009; Zhuang et al., 2011). However, detailed provenance interpretations of sediments in the Qaidam basin are relatively scarce, and the parent rocks and their spatial and temporal distributions in the source regions remain unclear. Through paleocurrent measurements and sandstone petrography, Ritts and Biffi (2001) proposed that Jurassic and Cretaceous sediments in the northeastern Qaidam have a derivation from the Qilian Shan. Based on petrography and geochemistry, Rieser et al. (2005) reported that only a slight variation occurred in the compositions of Cenozoic sandstones in the northwest sector of the Qaidam basin. They also reported numerous $^{40}Ar/^{39}Ar$ ages of detrital white mica from Cenozoic sediments, and suggested a northern (Altun Mountains) and/or southern (Qimantagh–Kunlun Mountains)

* Corresponding author at: MOE Key Laboratory of Orogenic Belts and Crustal Evolution, School of Earth and Space Sciences, Peking University, Beijing, 100871, PR China. Tel.: +86 10 62754113.
E-mail addresses: xjian@pku.edu.cn (X. Jian), pguanl@pku.edu.cn (P. Guan).

0037-0738/$ – see front matter © 2013 Elsevier B.V. All rights reserved.
http://dx.doi.org/10.1016/j.sedgeo.2013.03.010

provenance for the western Qaidam basin (Rieser et al., 2006a). The data of detrital mica from the Lulehe Section in the eastern Qaidam basin revealed a uniform Permian source (Rieser et al., 2006b). Additional research, such as precise provenance analysis based on sensitive approaches, is needed to acquire a greater understanding of the provenance of sandstones in the northern Qaidam basin.

Sandstone provenance can be determined by a variety of methods, including framework grain composition analysis, heavy mineral analysis, whole-rock geochemistry, mineral chemistry and radiometric dating (Weltje and von Eynatten, 2004; Najman, 2006). Sedimentary petrography is a classical and standard method in provenance studies. Data collected by point counting in sandstone thin sections often provide initial insight for provenance determination. Discrimination diagrams have been constructed from well known tectonic settings and provenances to interpret clastic deposits for a particular time, setting and location on earth (Dickinson and Suczek, 1979; Ingersoll and Suczek, 1979; Ingersoll et al., 1984; Dickinson, 1985; Zuffa, 1985). Heavy mineral analysis is one of the most sensitive and effective tools for sandstone provenance discrimination. Many minerals have very specific geneses that can provide crucial provenance information (Morton, 1985; Morton and Hallsworth, 1994, 1999). To overcome the influences of alteration during the entire sedimentation and diagenesis cycle, Morton and Hallsworth (1994) proposed a number of provenance-sensitive heavy mineral ratios (e.g., apatite–tourmaline index (ATi), garnet–zircon index (GZi)), most of which are widely applied in sandstone provenance analysis (e.g., Hallsworth et al., 2000; Morton et al., 2004, 2005; Hallsworth and Chisholm, 2008). Currently, mineral chemistry of a single mineral group is readily applied in many provenance studies. Detrital garnet and tourmaline, which are comparatively abundant and stable in sandstones, are frequently used as provenance indicators (e.g., Sabeen et al., 2002; Morton et al., 2004, 2005; Mange and Morton, 2007; Win et al., 2007; Hallsworth and Chisholm, 2008; Takeuchi et al., 2008; Morton et al., 2009; Meinhold et al., 2010).

However, in some case studies, a single technique is insufficient for solving a provenance problem; significant detail is lost when only one technique is applied. Morton et al. (2012) advocated the importance of adopting an integrated approach, to overcome the limitations associated with individual approaches. An integrated approach can also establish a more comprehensive representation of source area characteristics.

This paper aims to provide the results and provenance interpretations of the Tertiary sandstones in the northern Qaidam basin by combining detrital framework grain composition, heavy mineral data and mineral chemical data. The purpose of the paper is twofold: the first objective is to reconstruct the source parent rock types and their spatial and temporal distributions; the second objective is to provide additional data regarding tectonic history of the northern Tibetan Plateau.

2. Geologic setting and samples

2.1. Geologic setting

The rhomb-shaped Qaidam basin is a large intracontinental sedimentary basin that is located on the northeastern corner of the Tibetan Plateau in northwestern China (Fig. 1a). The area of the basin is approximately 120,000 km^2. It is situated approximately 2.7–3.0 km above sea level and has developed a thick Mesozoic to Cenozoic sedimentary succession of 3–16 km, with an average of 8 km. The basin is bounded by three large mountain ranges. The Kunlun Mountains are located to the south, the Qilian Mountains are along the east, and the Altun Mountains are located to the northwest (Fig. 1a).

The formation of the Qaidam basin is considered the result of the convergent system at the northern margin of the Tibetan Plateau (Tapponnier et al., 2001). It is closely related to the India–Asia collision, and is associated with the rise, thickening, shortening and lateral extrusion of the Tibetan Plateau (Harrison et al., 1992; Tapponnier et al., 2001; Yin et al., 2002; Yue et al., 2003). Consequently, a series of thrust fold belts in the northwest-southeast direction in the basin and reverse faults along the Kunlun Mountains and Qilian Mountains developed.

The northern Qaidam basin is approximately 30,000 km^2. It extends approximately 200 km from west to east and extends approximately 150 km from north to south (Fig. 1b). The northern Qaidam basin can be divided into many sections based on internal deformation. To simplify the discussion of the depositional areas in the study, it is divided into three fold belts, namely the Lenghu, Maxian, Eboliang fold belts and five depressions, namely the Yiliping, Kunteyi, Qianxi, Yuka and Suganhu depressions. The Lenghu fold belt is divided into five units: No. 3, No. 4, No. 5, No. 6 and No. 7 Lenghu fold belts. The Maxian fold belt is divided into three units: the Mahai, Beilingqiu and Nanbaxian fold belts.

The North Qaidam, South Qilian terranes and the southern flanks of the Altun Mountains are the adjacent source regions of the northern Qaidam basin. The North Qaidam terrane, which extends in the northwest direction between the Qaidam basin and Qilian block, is represented by a Paleozoic metamorphic belt with exhumed rocks dominated by shallow-marine strata, mélange and granite, as well as granitic and pelitic gneisses with lesser amounts of eclogite and garnet peridotite (Gehrels et al., 2003; Song et al., 2003a,b, 2005; Mattinson et al., 2006; Song et al., 2006; Yang et al., 2006; Mattinson et al., 2007; Song et al., 2007a,b; Zhang et al., 2008a; Mattinson et al., 2009; Menold et al., 2009). The South Qilian terrane is a metamorphic belt with Upper Proterozoic–Lower Paleozoic metamorphic rocks (Gehrels et al., 2003). To the west, the southern flanks of the Altun Mountains consist of granites, metamorphic complexes, Jurassic rocks and Ordovician rocks; whereas to the east, the Altun mountains consist of Paleozoic and Mesozoic granites and a few diorites predominate with metamorphic rocks of different grades from the Proterozoic Dakendaban Group (Gehrels et al., 2003; Yang et al., 2006; Mattinson et al., 2007).

2.2. Stratigraphy of Qaidam basin

Cenozoic sedimentary strata in the Qaidam basin consist of continental sedimentary facies. The sedimentary succession was deposited mainly in a fluvial–lacustrine environment, including the alluvial fans (mainly conglomerates) along the basin margins, and fluvial, delta and lake sediments (sandstones, siltstones and mudstones), which are widespread throughout the basin fill. Lake sediments are divided into near-shore and deep-water sediments with many thin layers of carbonates. Various evaporites (gypsum and halite) formed during regressive phases of lake development, primarily in the Late Miocene to Pleistocene (Unpublished data).

Based on the basin-wide lithostratigraphic framework, the microfossil studies, magnetostratigraphy and isotope geochronology (Ye et al., 1993; Sun et al., 2005; Wang et al., 2007), the Cenozoic strata of the Qaidam basin can be divided into 7 stratigraphic units (Fig. 2) compared with distinct seismic reflectors (T_0–T_5 in Fig. 2). These units are listed as follows (in ascending order, Fig. 2): (1) Lulehe Formation (Paleocene to early Eocene, ?–~45 Ma); (2) Xia Ganchaigou Formation (middle to late Eocene, ~45–~35.5 Ma); (3) Shang Ganchaigou Formation (late Eocene to Oligocene, ~35.5–~22 Ma); (4) Xia Youshashan Formation (early to middle Miocene, ~22–~15 Ma); (5) Shang Youshashan Formation (middle to late Miocene, ~15–~8 Ma); (6) Shizigou Formation (late Miocene to Pliocene, ~8–2.8 Ma); and (7) Qigequan Formation (Quaternary, 2.8 Ma–present). Based on field outcrop and core drilling investigation in the northern Qaidam basin, Lulehe Formation strata are predominantly composed of alluvial fan deposits. Fluvial, delta and lake sediments are widely distributed from the Xia Ganchaigou Formation to the Shang Youshashan Formation. The strata from the upper Shang Youshashan Formation to the Qigequan Formation are composed of alluvial fan facies.

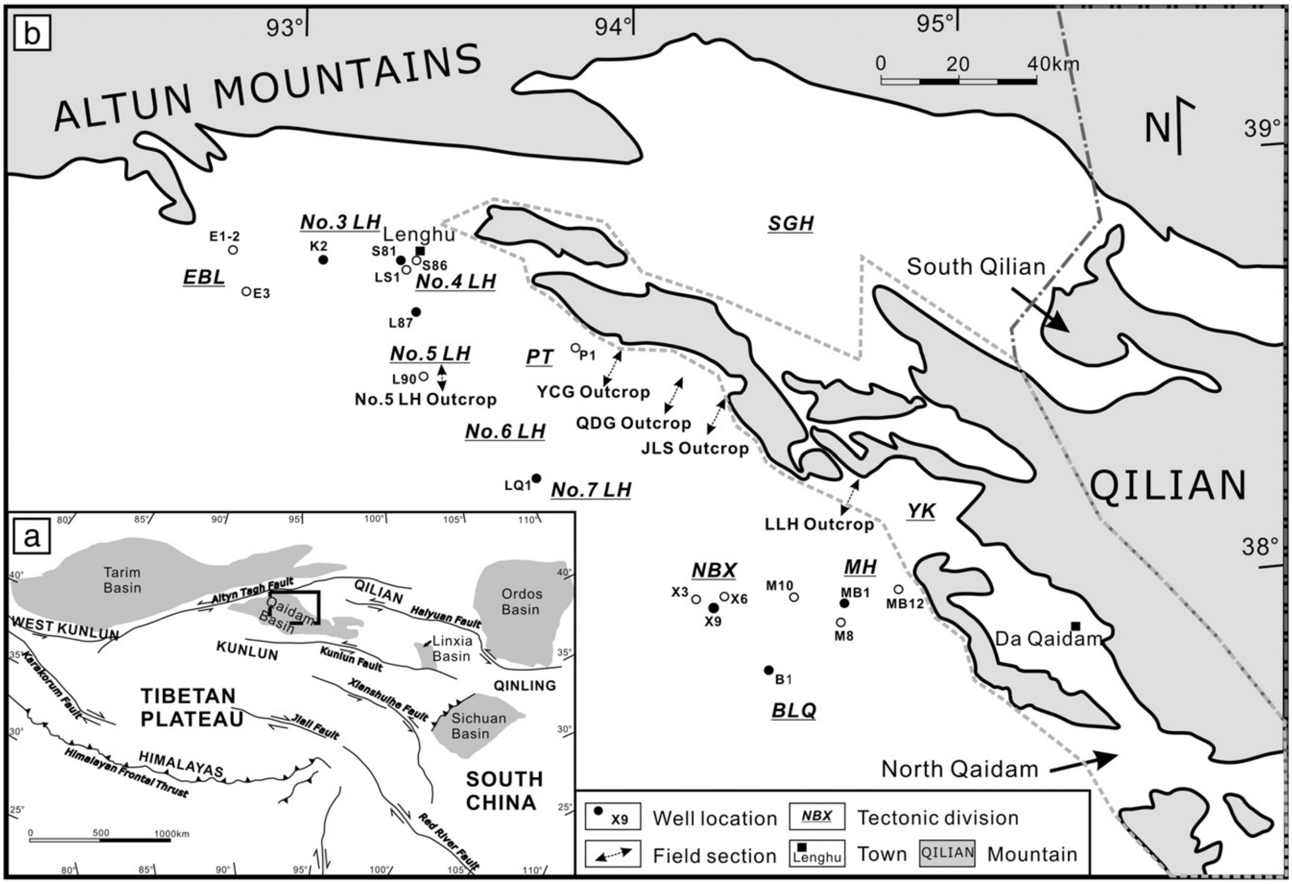

Fig. 1. Geological setting of Qaidam basin and study area. (a) Location of the Qaidam basin at the northeastern margin of the Tibetan Plateau (modified from Tapponnier et al., 2001). The rectangle depicts the outline of b. (b) Locations of the main investigated wells and outcrops. SGH: Suganhu, YK: Yuka, PT: Pingtai, BLQ: Beilingqiu, MH: Mahai, NBX: Nanbaxian, No. 3 LH: No. 3 Lenghu, EBL: Eboliang, No. 4 LH: No. 4 Lenghu, No. 5 LH: No. 5 Lenghu, No. 7 LH: No. 7 Lenghu, No. 5 LH Outcrop: No. 5 Lenghu Outcrop, YCG Outcrop: Yingchaogou Outcrop, QDG Outcrop: Quandonggou Outcrop, JLS Outcrop: Jielusu Outcrop, LLH Outcrop: Lulehe Outcrop.

2.3. Sample description

The sandstone samples in this study were collected from 5 outcrops and 19 drilling wells in the northern Qaidam basin (Fig. 1b; Table A.1, in Appendix A online). The samples represent the Lulehe Formation to the Shizigou Formation. The majority of the samples are composed of fluvial and delta sediments, although a small minority of samples derive from sand bodies in alluvial fan and near-shore lake facies (Table A.1, in Appendix A online). The location, depth and lithology of each sample are shown in Figs. A1 and A2 (in Appendix B).

3. Methods

3.1. Framework petrography

Approximately 150 sandstone samples were ground to thin sections. Their petrography features, including mineral constituents, grain size, sorting and roundness, were observed using a polarization microscope and recorded. Modal analyses of 75 selected sandstone samples were performed on each thin section, using the Gazzi–Dickinson method (Dickinson, 1985). Medium- to coarse-grained sandstones were used for point counting to minimize grain-size effects (Ingersoll et al., 1984). A minimum of 400 points were counted per sample.

3.2. Heavy mineral analysis

A total of 92 sandstone samples were selected and examined through heavy mineral analysis. Each sandstone sample, which weighed 1–2 kg, was selected from fresh medium- to coarse-grained sandstones with an average grain size greater than 0.2 mm. Separation and preparation of the heavy minerals were performed by following standard procedures described by Mange and Maurer (1992). The detailed heavy mineral analysis process was described by von Eynatten and Gaupp (1999) and Li et al. (2004).

3.3. Mineral chemistry

Detrital garnet and tourmaline grains were separated from selected sandstone samples, adhered to targets using epoxy resins, and ground and polished for electron probe micro-analyzer (EPMA) analyses. The chemical compositions of detrital garnets and tourmalines were analyzed using a JEOL JXA 8100 electron-microprobe at Peking University. Forty grains per sandstone sample were randomly analyzed at the grain core part. A total 640 garnets in 16 samples and 160 tourmalines in 4 samples were analyzed in this study. The operating conditions are shown in studies by S. Song et al. (2007) and Zhang et al. (2008a). The chemical calculation and classification of tourmalines were achieved using the CLASTOUR program (Yavuz et al., 2002).

3.4. Log-ratio statistical analysis

Multivariate statistical methods, which have been developed and used to treat compositional data in provenance analysis (e.g., Weltje, 2002; Garzanti et al., 2005, 2006; Weltje, 2006; Ingersoll and Eastmond, 2007; Allen and Johnson, 2010), were applied to evaluate the ternary compositional data of detrital framework grains and heavy mineral assemblages in this study. The details were reviewed by Weltje (2002). This method is based on the log-ratio transformation (Aitchison, 1986)

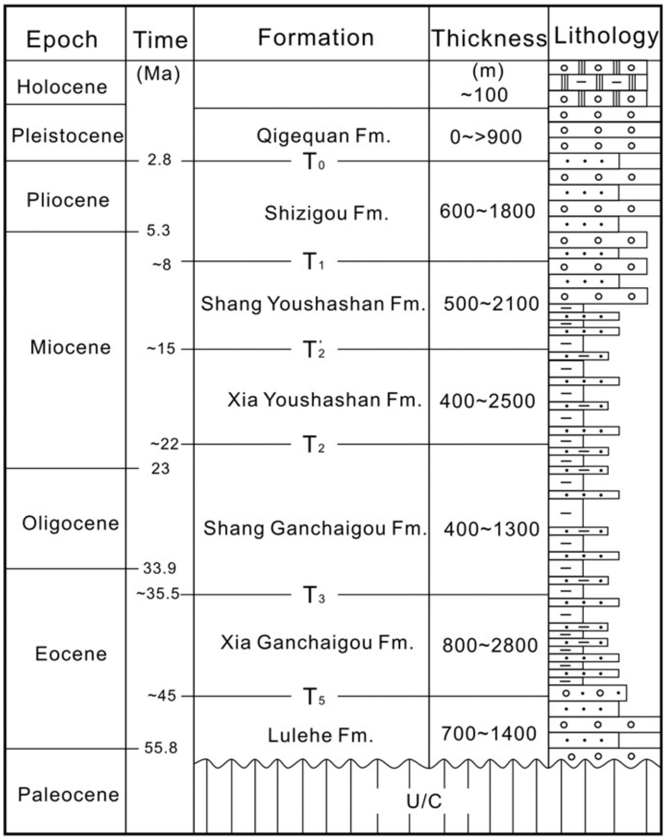

Fig. 2. Cenozoic stratigraphy, seismic reflectors (T_0–T_5), thickness and representative lithological column of the northern Qaidam basin.

and removes statistical constraints on compositional variables, including non-negativity and the constant-unit sum (Weltje, 2012). References for the mathematical foundations of log-ratio transformation include Aitchison (1986), Egozcue et al. (2003) and Tolosana-Delgado (2012). CoDaPack3D software (Comas-Cufí and Thió-Henestrosa, 2011) was employed to obtain the confidence region ellipsoids for the population mean. Detailed equations for calculating the boundary of the multivariate confidence region ellipsoids are discussed in studies by Weltje (2002) and Ingersoll and Eastmond (2007). In this study, multivariate geometric means and corresponding 95% confidence ellipsoids (for populations with sample sizes >3) were calculated and illustrated in ternary diagrams.

Note that log-ratio compositional data analysis provides rigorous confidence regions when used to treat sample groups with a certain amount of data, whereas small sample sizes of the dataset significantly increase confidence fields (Weltje, 2002; Ingersoll and Eastmond, 2007; Allen and Johnson, 2010). Weltje (2002) interpreted these large confidence region ellipsoids for small populations as the result of uncertainties. Therefore, the confidence ellipsoids for populations of small sample sizes are less significant; conversely, the ellipsoids for larger sample sizes are more significant.

4. Sandstone framework petrography

4.1. Texture and composition

Most of the detrital grains of the Tertiary sandstones are angular to subangular and poorly to moderately sorted (Fig. 3B–D). They can be interpreted as first-cycle sandstones with short transport distances. Some sandstones (e.g., samples from Nanbaxian and Beilingqiu) are present with subrounded to rounded and well-sorted grains dominated by quartz (Fig. 3A and E), which suggests recycling and/or relatively long transport distances. The sandstones contain abundant lithic fragments (Table A.2, in Appendix A online), which are mainly constituted by sedimentary and metasedimentary lithic fragments, including carbonate, chert, phyllite, schist, and metaquartzite (e.g., Fig. 3C–D). Feldspars composed of plagioclase and K-feldspar, are present in relatively low abundance, whereas samples of No.3 Lenghu display high feldspar abundance (e.g., Fig. 3B).

4.2. Detrital modal analysis

The point-count data of Sandstone thin section and results of the modal analysis are presented in Table A.2 (see Appendix A online) and Fig. 4. Table A.2 also presents the average compositions and standard deviations of sandstones from each area. The results are illustrated in framework grain assemblage Q-F-L and Qm-F-Lt, and in framework lithic grain Qp-Lsm-Lvm diagrams (Dickinson, 1985).

Overall, quartz is the relatively abundant component in these samples (Figs. 4–5; Table A.2, in Appendix A online), with abundances (in Q-F-L diagram) ranging from 36% to 74% (arithmetic mean of 54 ± 9% for all 75 samples from the Tertiary successions). Monocrystalline quartz is considerably more plentiful than polycrystalline quartz, with averages of 49% and 5%, respectively. Lithic fragments, excluding polycrystalline quartz and carbonate, range from 8% to 51% (arithmetic mean of 29 ± 10%) in the ratios. These lithic fragments are mainly of metamorphic source constituted by different types of low-grade metamorphic rocks (e.g., schist and phyllite, Fig. 3C–D), whereas sedimentary lithic fragments (e.g., chert) are subordinate and only a few volcanic fragments are found in the samples (Fig. 5c). Feldspars dominated by plagioclase constitute an average of 17 ± 8% of Qm-F-Lt framework grains (Table A.2, in Appendix A online), with a range of 4 to 37%. The compositional data of all but two samples suggests a recycled orogen provenance of the sandstones (Fig. 4a). However, these samples are plotted as quartzose recycled, transitional recycled and mixed sources on the Qm-F-Lt ternary diagram (Fig. 4b). In the Qp-Lvm-Lsm ternary diagram, these samples mainly plot near the Lsm pole, which indicates a derivation of collision suture and fold-thrust belt sources (Fig. 4c).

The average framework grain compositions display slight variations for sandstones from different areas (Table A.2, in Appendix A online; Figs. 5 and 6). Samples of the Mahai, Beilingqiu, Nanbaxian and Eboliang fold belts exhibit similar average compositions (Fig. 5) and are characterized by relatively high quartz contents (in excess of 50%). The average abundances of Qm, F and Lt of these samples are 51 ± 6:15 ± 6:34 ±6, 55 ± 12:15 ± 4:30 ± 16, 54 ± 9:14 ± 5:32 ± 13 and 55 ± 5:17 ± 1:28 ± 7, respectively. However, samples of the No. 5 Lenghu fold belt and Yingchaogou outcrop exhibit relatively low quartz and high lithic fragment contents (Fig. 5). Their average abundance ratios of Qm, F and Lt are 47 ± 8:14 ± 3:38 ± 10 and 47 ± 11:16 ± 9:36 ± 13. The samples from No. 3 Lenghu and No. 4 Lenghu fold belts exhibit relatively high feldspar contents (Figs. 3 and 5), as with Sample K2-03 (maximum feldspar abundance of 35%). The average abundance ratios of Qm, F and Lt from the samples of these two areas are 45 ± 3:33 ± 2:22 ± 5 and 43 ± 5:23 ± 5:34 ± 7. Only one sample was collected from No.7 Lenghu. The ratio of Qm:F:Lt is 46:25:29. In these analyzed sandstones, lithic fragments are mainly composed of metamorphic lithic fragments with subordinate volcanic and sedimentary lithic fragments (Fig. 5c). Samples from No. 3 Lenghu display a relatively high abundance of volcanic lithic fragments (Fig. 5c).

5. Heavy mineral analysis

5.1. Heavy mineral assemblages

The heavy mineral analysis data are listed in Table A.3 (see Appendix A online). Overall, the heavy mineral spectra of the analyzed sandstones (n = 92) are primarily dominated by hematite, with an average of 25% (maximum 82.5%, Table A.3, in Appendix A online). Hematite is the

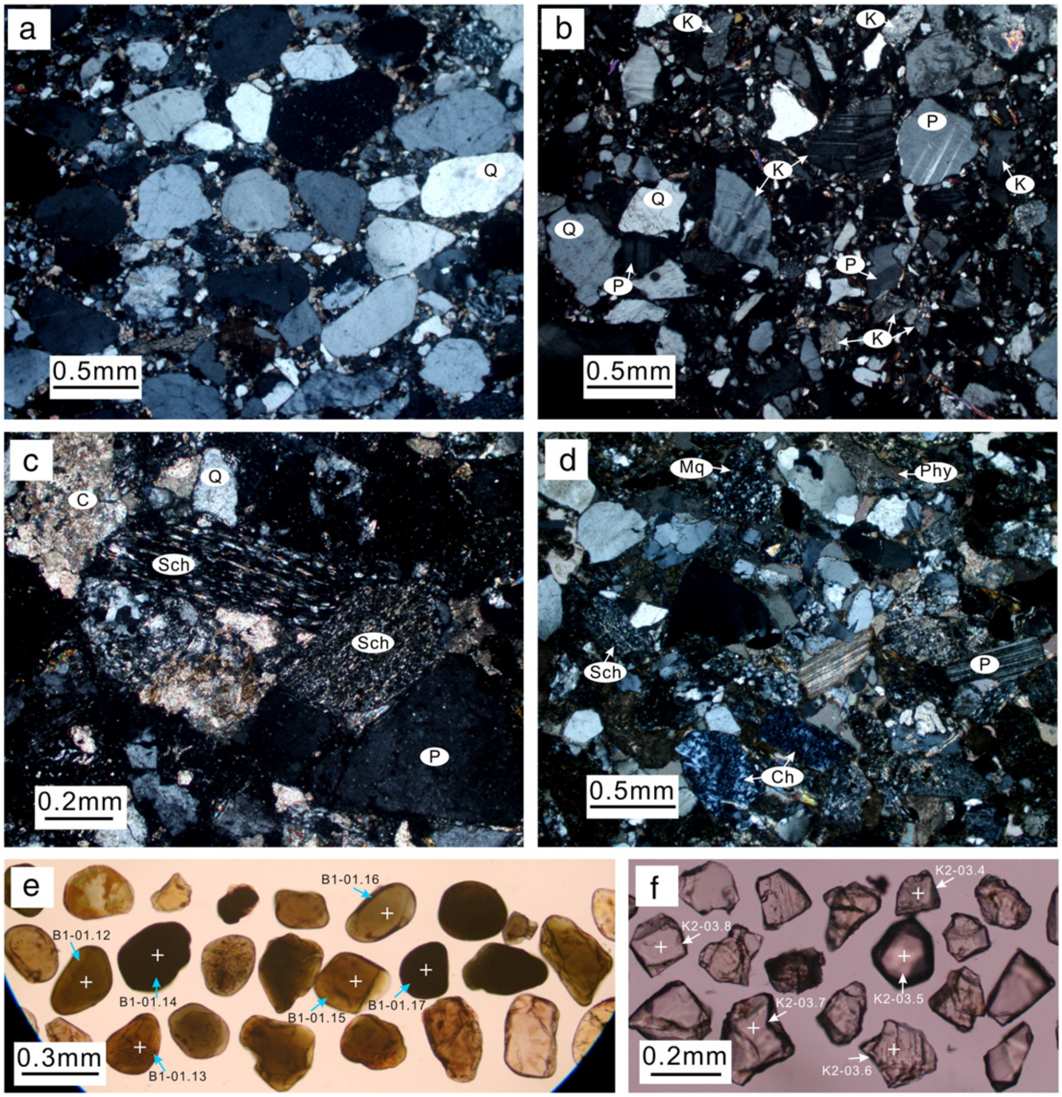

Fig. 3. Representative photomicrographs of the Tertiary sandstones and heavy minerals. A) Quartzose arkose with subrounded to rounded grains (Sample B1-02). B) Lithic feldspathic sandstone with high feldspar abundance, including both plagioclase (P) and K-feldspar (K) (Sample K2-03). C) Lithic sandstone with schist (Sch) and carbonate (C) fragment enrichment (Sample YCG-19). D) Lithic sandstone rich in various lithic fragments, e.g., schist (Sch), chert (Ch), phyllite (Phy) and metaquartzite (Mq) (Sample S86-01). E) Tourmaline grains for EPMA analysis (the target of Sample B1-01), most of the grains are rounded. F) Angular to subangular shaped garnet grains for EPMA analysis (the target of Sample K2-03). All photomicrographs were taken with cross-polarized light, with the exception (E) and (F). The white cross marks in (E) and (F) are the EPMA analysis spots, and the text (e.g., B1-01.13, K2-03.6) adjacent to the marks represent the analysis numbers.

oxidation product of pyrite, magnetite or other iron-bearing minerals during weathering, abrasion, transport and deposition. Garnet and epidote exhibit the significant contents, with averages of 22.1% (maximum 68.9%) and 18.8% (maximum 58.6%), respectively. This mineral group is mainly derived from metamorphic source rocks with various grades, whereas epidote is particularly common in rocks of greenschist and epidote–amphibolite facies (Deer et al., 1992). The stable detrital heavy mineral assemblage of high mineralogical maturity, which is primarily composed of zircon, tourmaline and rutile (Morton, 1985; Morton and Hallsworth, 1999), display a range of 0.3% to 44% with an average of 9.9%. This mineral assemblage is common in acidic to intermediate granitoid rocks, as well as in mature siliciclastic sediments and some metamorphic rocks. In most analyzed samples, zircon displays the highest concentration of ZTR (zircon > tourmaline > rutile) minerals. Ilmenite, which is often derived from basic, acidic rocks and pegmatites, comprises an average of 7.6% of the total heavy mineral assemblage. Other heavy minerals, e.g., leucoxene, anatase, apatite and titanite, are found in most samples, but often show low contents (with averages less than 5%). In addition, magnetite, spinel, chlorite, kyanite, pyroxene and hornblende serve as minor constituents and exhibit low abundances (Table A.3, in Appendix A online). Figs. 7 and 8 show the average heavy mineral abundances and the corresponding confidence regions of samples grouped by locations.

The heavy mineral assemblages of samples from Mahai, Beilingqiu, Nanbaxian and No. 7 Lenghu have similarities that are dominated by hematite, ZTR minerals, garnet and leucoxene (Fig. 7a). Twenty-two sandstones from these 4 locations show variable concentrations of hematite (ranging from 0.5% to 60.1%, with an average of 23.3 $\pm$ 18.5%), but display relatively high ratios of ZTR minerals (maximum 44.4%, Sample X9-18 of Nanbaxian), with averages of 21.6%, 17.6%, 24.9% and 29.2%. This observation is supported by ZTR index and stability index. Sandstone samples from these locations yield high ZTR and stability indexes (Fig. 9a). Garnet and leucoxene also comprise certain proportions of the total heavy mineral assemblages, with averages of 18.7% and 10.0%, respectively. Minor components are comprised of apatite, titanite and epidote.

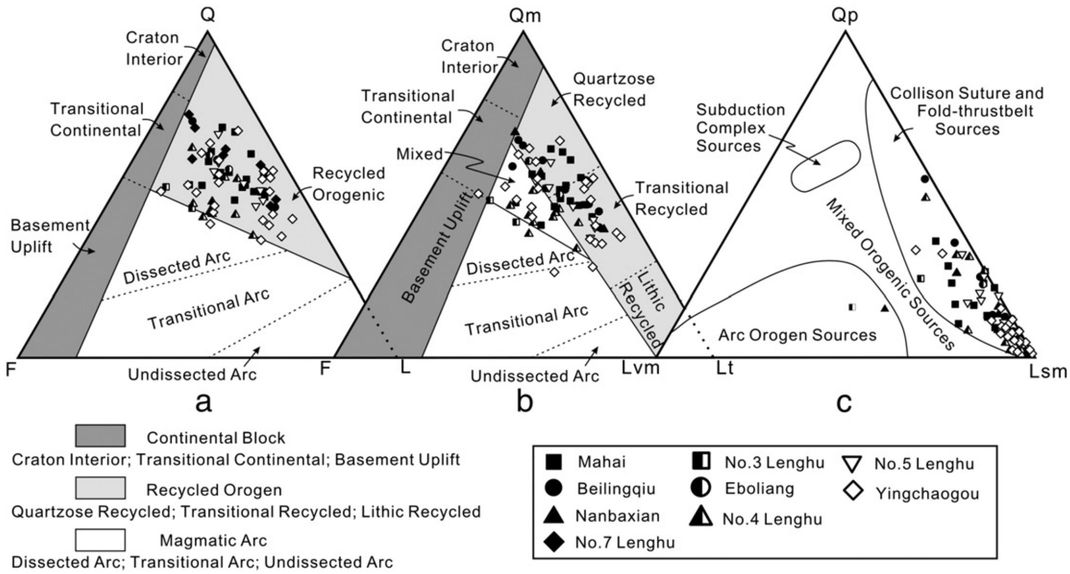

Fig. 4. Triangular plots of sandstone framework grain compositions. (a) Q-F-L diagram; (b) Qm-F-Lt diagram; (c) Qp-Lvm-Lsm diagram. Provenance fields are from Dickinson (1985). For data and abbreviations see Table A.2 (in Appendix A online).

The heavy mineral assemblages of samples from No. 5 Lenghu and the Yingchaogou, Quandonggou and Jielusu outcrops are characterized by high epidote and garnet abundances, with averages of 33.8% and 17.4% (Fig. 7b). Hematite is also one major mineral phase, but it is comprised of different concentrations in these samples. Sandstone samples from No.5 Lenghu exhibit high abundances of ilmenite, with an average of 16.3% (Table A.3, in Appendix A online). Note that there is a notably low abundance of ZTR minerals in the sandstones from these four locations (Fig. 7b). Hence, they yield very low ZTR and stability indexes (Fig. 9a). Other species are mainly unstable detrital heavy minerals of low mineralogical maturity, including titanite, apatite, hornblende and pyroxene with low abundances. Hornblende (maximum 22.4%, Sample YCG-38) and pyroxene (maximum 11.7%, Sample QDG-05) mainly occur in samples from the Yingchaogou and Quandonggou outcrops, giving high ratios in the samples from strata of the Xia Youshashan and Shang Youshashan Formations (Table A.3, in Appendix A online).

Samples of Eboliang, No. 3 Lenghu and No. 4 Lenghu contain the highest abundances of hematite (Fig. 7c), with averages of 46.9%, 48.1% and 43.9%, respectively (Table A.3, in Appendix A online), followed by garnet and ZTR minerals. Sandstone samples of these three locations have relatively moderate ZTR and stability indexes (Fig. 9a). Furthermore, leucoxene, epidote, titanite and ilmenite comprise certain proportions of the total heavy mineral assemblages. Some samples display high contents of titanite (maximum 24.5%, Sample K2-03 of No. 3 Lenghu) or ilmenite (maximum 62.1%, Sample S81-01 of No. 4 Lenghu). Anatase and apatite serve as minor constituents.

Samples of Lulehe outcrop show high garnet and hematite abundances (Figs. 7a and 8a) with averages of 50.4% and 19.9%, respectively (Table A.3, in Appendix A online). Ilmenite shows variable contents in these analyzed samples. The heavy mineral assemblages of samples from Pingtai are characterized by high ilmenite, garnet and epidote abundances with subordinate hematite (Fig. 7b), which resemble samples from No. 5 Lenghu.

5.2. Heavy mineral ratios

According to the relatively high abundances of garnet, epidote and ZTR minerals in the analyzed samples, the ratios of GZi, rutile/zircon (RuZi) and epidote/titanite (ETi) are recommended to reflect and compare provenance characteristics in this study (Table A.3, in Appendix A online; Fig. 9b–d). GZi and RuZi are proposed by Morton and Hallsworth (1994), although low GZi values may be a result of either provenance or garnet dissolution. However, it has been proved useful in our research

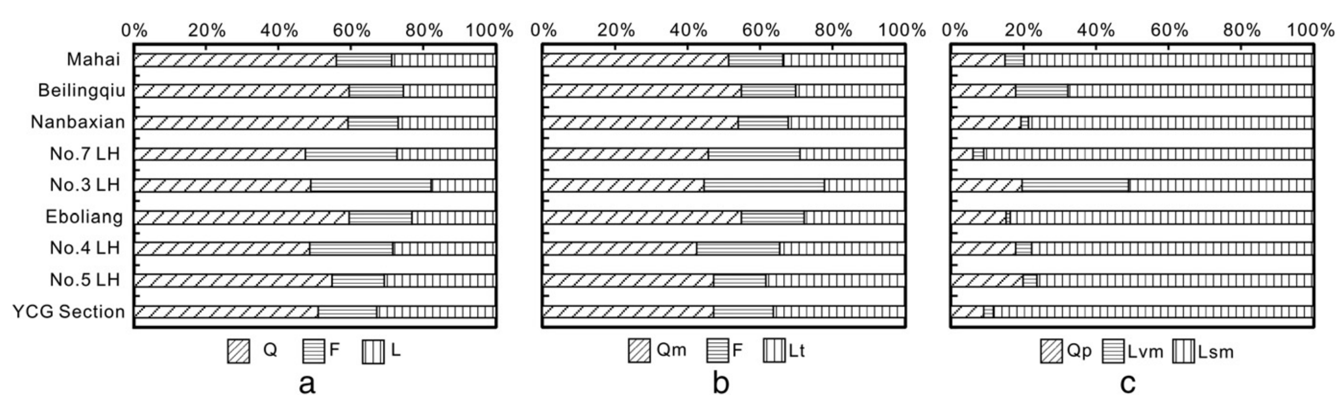

Fig. 5. Average framework grain compositions of sandstones from each location. For data, see Table A.2 in Appendix A online. (a) Q-F-L diagram; (b) Qm-F-Lt diagram and (c) Qp-Lvm-Lsm diagram. Note that arithmetic means are used.

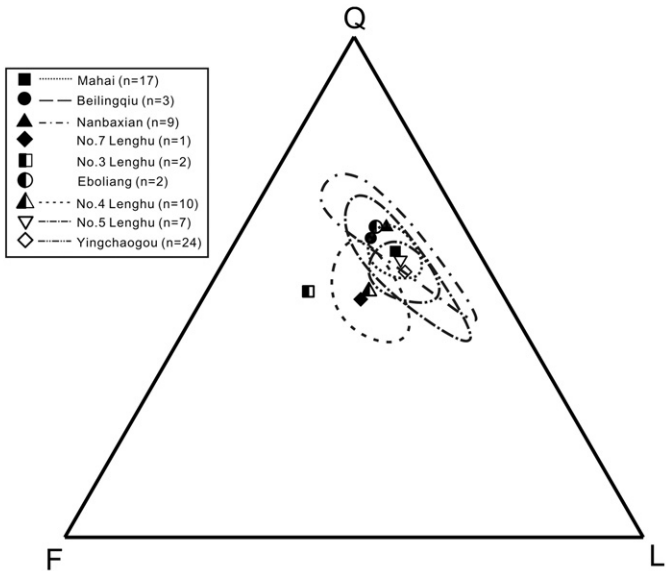

Fig. 6. QFL ternary diagrams showing spatial variation of detrital framework components of sandstones (grouped by locations). Geometric means and 95% confidence ellipsoids (only for sample groups with sample size n > 3) calculated using the log-ratio method (Weltje, 2002). Note that the provenance tectonic settings were removed in the QFL diagram because geometric means and confidence regions cannot be used to test the Dickinson's model (Ingersoll and Eastmond, 2007), which was created with untransformed data (Dickinson, 1985).

area. Consider Sample K2-01 (5242.8 m) and Sample K2-03 (3364 m) as examples, the deeper sample exhibits the higher GZi value (Table A.3, in Appendix A online). ETi (ETi = 100 × epidote abundance/total abundance epidote plus titanite) is defined in this study. Epidote and titanite display similar densities and stability of burial diagenesis (Morton and Hallsworth, 1999); hence, the ratio of epidote and titanite can be used in provenance analysis to minimize influences of hydraulic and diagenetic processes.

Fig. 9 presents the binary plots between heavy mineral ratios GZi, RuZi, ETi and the ZTR index, which reveal apparent variation among different locations. Sandstone samples of Mahai, Beilingqiu, Nanbaxian, No. 7 Lenghu, Eboliang, No. 3 Lenghu and No. 4 Lenghu are characterized by variable GZi (ranging from 7.2 to 95.5) and ETi (ranging from 0 to 100) values, as well as relatively low RuZi values (ranging from 2 to 31.1, with an average of 15.4). Samples of Pingtai, No. 5 Lenghu, Yingchaogou, Quandonggou and Jielusu outcrops display very high GZi (ranging from 65.3 to 97.6) and ETi (ranging from 47.9 to 99.7) values, with averages of 86.7 and 87.9, respectively, variable RuZi values, with a range varying from 6.3 to 54.5 (Table A.3, in Appendix A online; Fig. 9b–d). Samples of the Lulehe outcrop show high GZi values (with an average of 96.3), variable ETi values (ranging from 33.0 to 94.7, with an average of 73.6) and relatively low RuZi values (with an average of 18.8).

6. Mineral chemistry

6.1. Detrital garnet chemistry

The garnet group contains six end-members, including pyrope (Prp), almandine (Alm), spessartine (Sps), grossular (Grs), andradite (Andr) and uvarovite (Uva). The molecular percentage of each end-member of every analyzed garnet can be calculated once chemical compositions are obtained. Garnet is especially characteristic of metamorphic rocks of a wide variety of types. It can also be found in magmatic rocks such as

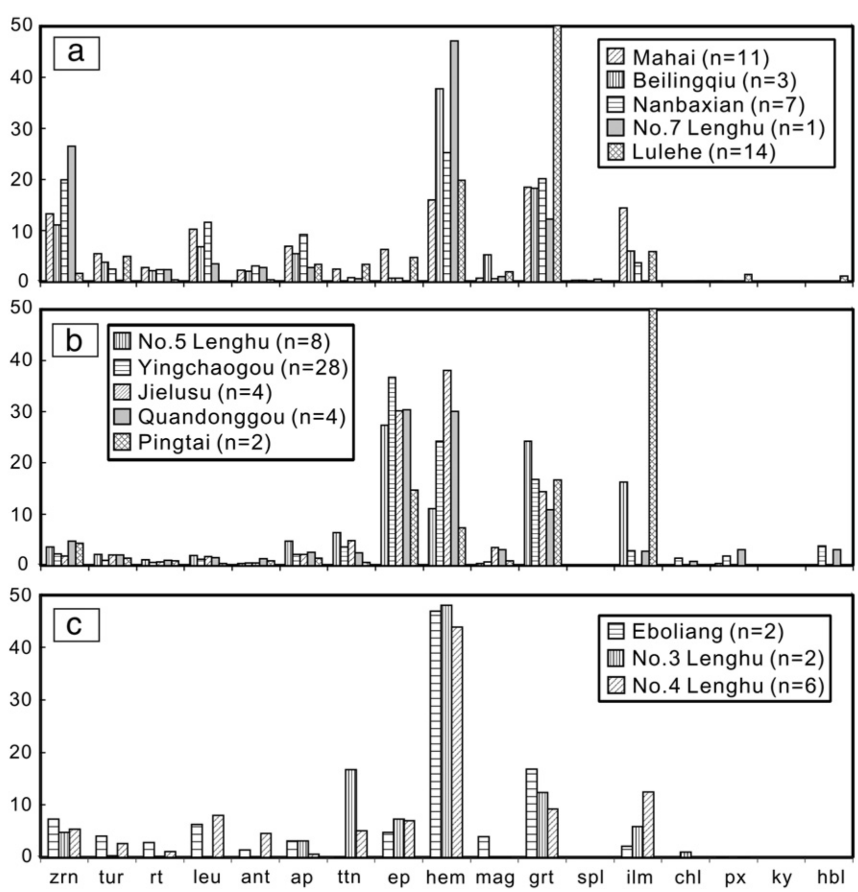

Fig. 7. Average heavy mineral assemblages of sandstones from each location. The data and abbreviations of heavy minerals are shown in Table A.3 (in Appendix A online).

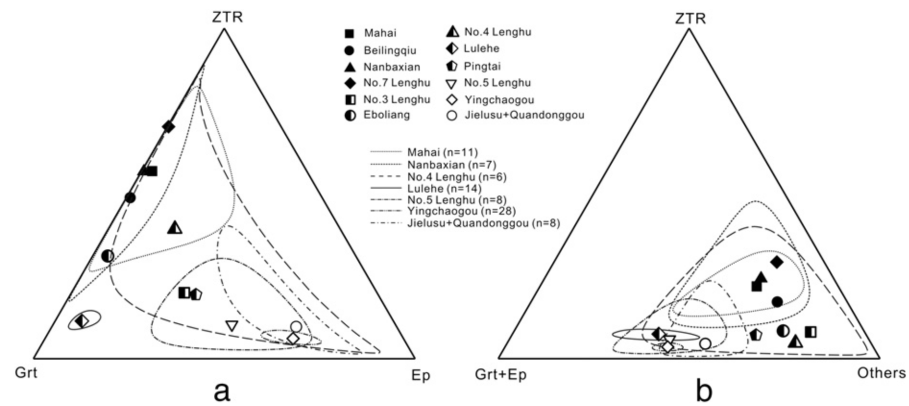

Fig. 8. Ternary diagrams displaying spatial variations of heavy mineral components of sandstones (grouped by locations). Geometric means and 95% confidence ellipsoids (n > 3) calculated using the log-ratio method (Weltje, 2002). ZTR: zrn + tur + rt; Grt: garnet; Ep: epidote; Others: leu + ant + ap + ttn + hem + mag + spl + ilm + chl + px + ky + hbl.

granites, pegmatites, acidic volcanic rocks, kimberlites and some metasomatic rocks (Deer et al., 1992).

Morton et al. (2004) distinguished three major detrital garnet types in sediments by construction of a ternary diagram of Prp-Alm + Sps-Grs + Andr (namely, Mg–Fe^{2+} + Mn–Ca) for source rock discrimination (Fig. 10a). The detrital garnets can be divided into three types, namely, Type A, B and C. The details of chemical characteristics and potential parent rocks of each type were described by Morton et al. (2004). This ternary diagram was improved by Mange and Morton (2007).

Detrital garnets of the sandstone samples reveal a pale pink or red color under plane-polarized light and are mainly angular in shape (e.g., Fig. 3F). A calculation of end-members indicated that the garnets show marked variations in chemical compositions (Table A.4, in Appendix A online; Fig. 10a–b). The average component of the total detrital garnets from the Tertiary sandstones is shown as $Alm_{67\pm9}Prp_{14\pm7}Sps_{8\pm9}Grs_{10\pm9}Andr_{1\pm1}$. The ranges are 26–91 mol% for almandine, 1–43 mol% for pyrope, 0–45 mol% for spessartine, 0–44 mol% for grossular and 0–9 mol% for andradite; uvarovite end-member is poor in these garnets.

Overall, according to Morton's discrimination diagram, all analyzed sandstone samples display Type B garnet enrichment (Fig. 10c), with an abundance of 77.3%, followed by Type C and Type A, with abundances of 12.7% and 10%, respectively. The results of end-member calculations for each sandstone sample are shown in the ternary diagram (Fig. 10d). The relative abundances of Type A, Type B and Type C garnets in each sample are shown in the Type A-B-C ternary diagram (Fig. 10e). Fig. 10f shows abundances of garnets with spessartine >5% and abundances of the high-Mn garnet grains plotted in the Bi field of the ternary diagram (namely, the filled circles in the Bi field). All diagrams demonstrate spatial variations among these samples. Therefore, the variations in garnet group components can be used to accurately identify different sources and characterize the source rock lithology.

Fig. 10b displays the plot of typical garnets from potential source rocks in the Qilian Mountains and the Altun Mountains, as reported in previous references. Those rocks include garnet peridotites, eclogites,

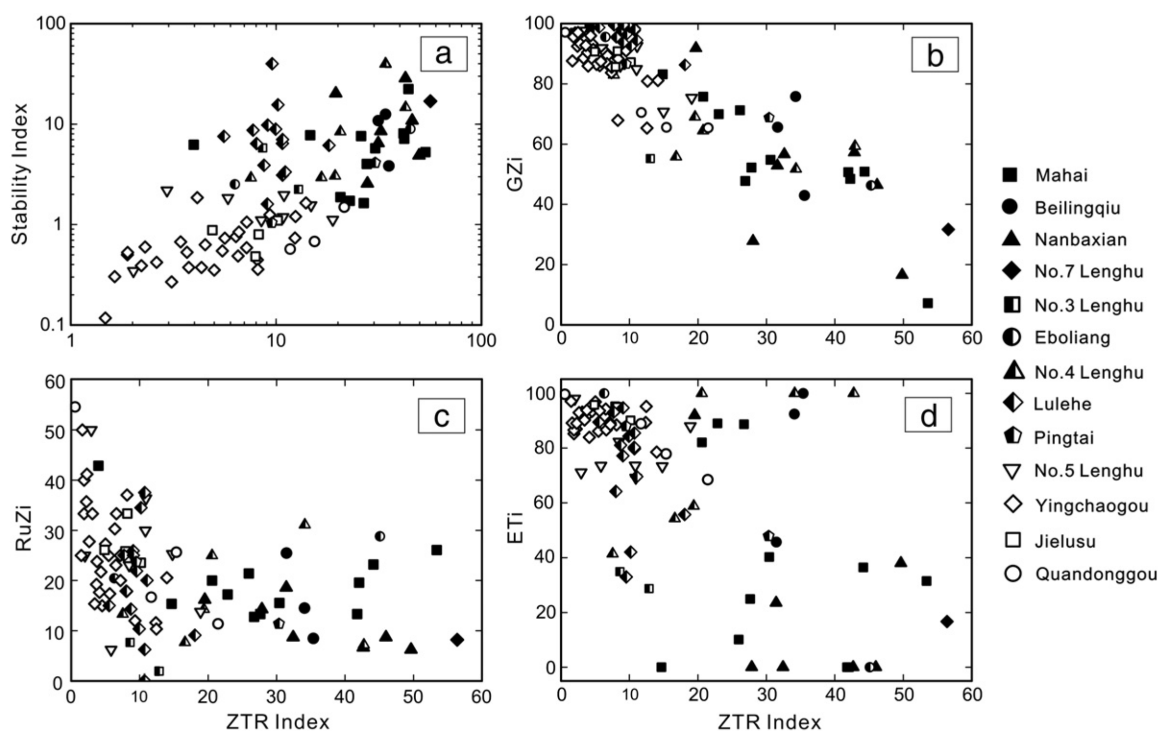

Fig. 9. Binary plot of heavy mineral stability indexes (ZTR and stability Indexes) and heavy mineral ratios (GZi, RuZi (Morton and Hallsworth, 1994) and ETi) showing spatial variation among different locations. For the data, see Table A.3 (in Appendix A online).

granulites, gneisses (including paragneisses and orthogneisses), amphibolites, and schists (including blueschists). However, the data of garnets from igneous rocks (e.g., granites) were not collected.

Most of the analyzed garnets of Samples YCG-02 and YCG-08 display as Type B garnet (67.5% and 55%, respectively); followed by Type C (32.5% and 42.5%, respectively). They exhibit relatively high contents of grossular components (Fig. 10d). The amount of Sps < 5% is greater than the amount of Sps > 5% for each sample (Fig. 10d, f). In the Type A-B-C ternary diagram (Fig. 10e), data from both samples are near to the Type B-C axis.

The detrital garnets of Samples YCG-17, YCG-30, YCG-38, JLS-19, L87-09, K2-03 and S81-01 are dominated by Type B garnet with traces of Type A and Type C garnets (Fig. 10d), therefore these samples are all in close proximity to the Type B apex in the Type A-B-C ternary diagram (Fig. 10e). However, the detrital garnets from these sandstone samples also reveal differences in compositions. The detrital garnets of

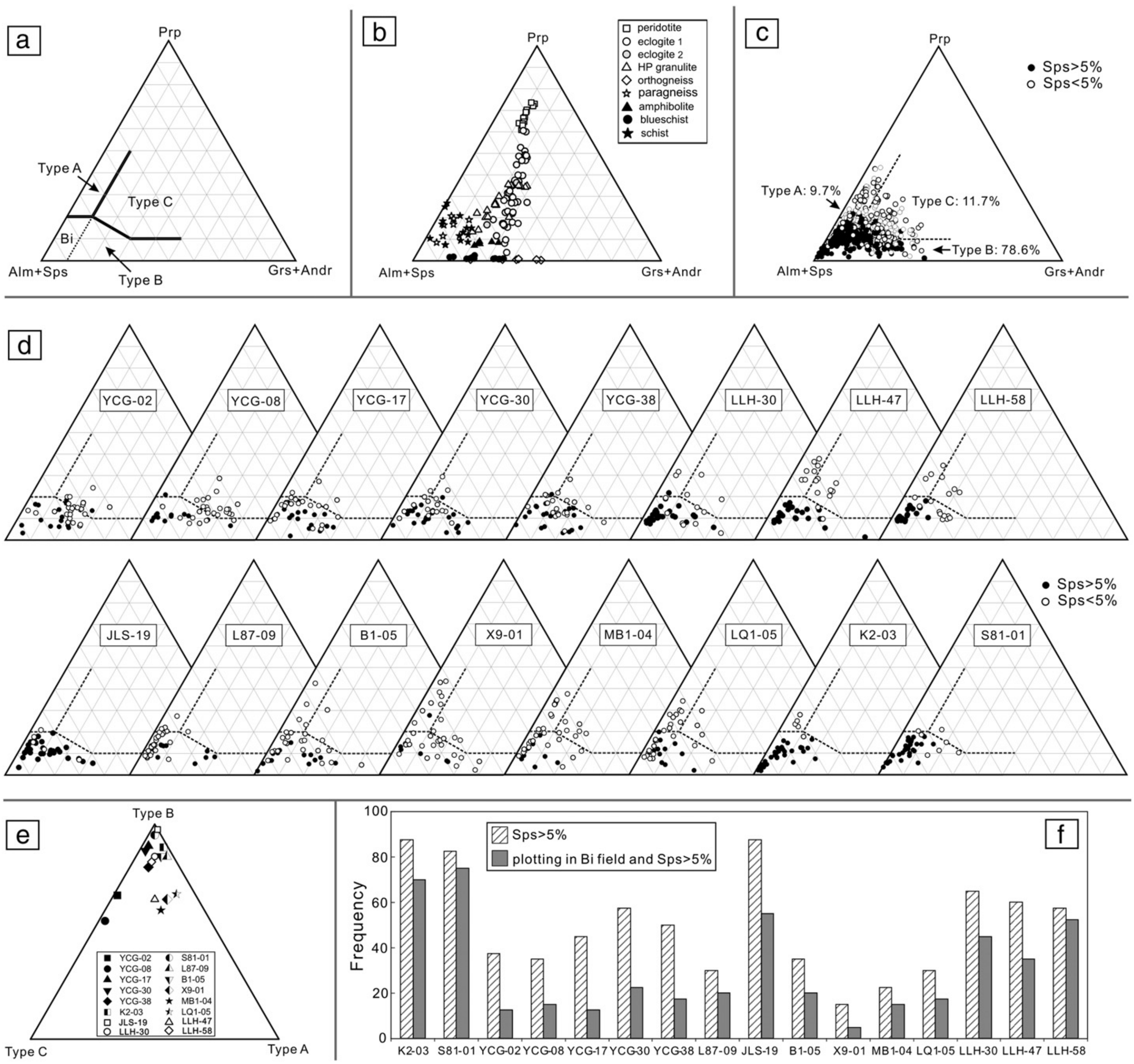

Fig. 10. Detrital garnet chemistry of selected sandstones. (a) Type A, B and C fields in the ternary diagram of Prp-Alm + Sps-Grs + Andr defined by Morton et al. (2004), of which the Bi field was proposed by Mange and Morton (2007); (b) Diagram showing the typical garnet compositions of the potential source rocks in the Qilian Mountains and the western segment of the Altun Mountains; (c) Ternary plot of detrital garnet chemical compositions in 16 Tertiary samples; (d) Ternary plots of detrital garnet compositions in each sandstone sample; (e) Relative abundances of Type A, B and C garnets for each analyzed sample; (f) the frequencies of garnet grains with greater than 5% Sps (in molecular proportions) and percentages of high-Mn garnet grains plotted in the Bi field. In diagram (b), the garnet peridotite data are from Song et al. (2007a); the eclogite data are from Zhang et al. (2001, 2005), and Zhang et al. (2008a, 2009a), the "eclogite 1" are from Qilian Mountains, whereas the "eclogite 2" are from the Altun Mountains; the High Pressure granulite data are from Zhang et al. (2007) and Yu et al. (2010); the orthogneiss data are from Menold et al. (2009); the paragneiss data are from Zhang et al. (2008b, 2009b); the blueschist data are from Liu et al. (2006) and Zhang et al. (2009c); the amphibolite data are from Zhang et al. (2009a), the schist data are from Zhang et al. (2000, 2004), Song et al. (2007b) and Song et al. (2009), and all samples are from the Qilian Mountains with the exception of the "eclogite 2". The abbreviations of end-members are show in Table A.4 (in Appendix A online). For representative data of detrital garnets, also see Table A.4 (in Appendix A online).

Samples JLS-19, YCG-17, YCG-30 and YCG-38 are characterized by variable grossular and pyrope contents. For each sample (except Sample JLS-19), the analyzed garnets, which show Sps < 5% and Sps > 5% are approximately equivalent (Fig. 10d, f). The majority of detrital garnets from Sample L87-09 exhibit relatively low grossular and spessartine contents and variable pyrope contents (Fig. 10d). The majority of detrital garnets from Samples K2-03 and S81-01 can also be classified as Type B garnets (Fig. 10d), but they are characterized by high-Mn abundance (Fig. 10f), with average spessartine end-member contents of 15.5% (maximum 32.1 mol%, and 87.5% of the total analyzed grains for Sps > 5%) and 13.2% (maximum 36.4 mol%, and 82.5% of the total analyzed grains for Sps > 5%), respectively. Therefore, numerous grains with greater than 5% Sps exist in the Bi field in the ternary diagram (Fig. 10d, f).

The detrital garnets of Samples X9-01, MB1-04 and LQ1-05 are dominated by Type B garnet with subordinate Type A and Type C garnets, and garnets of Sps < 5% are greater than the detrital garnets with Sps > 5% for each sample (Fig. 10d). These three sandstone samples are characterized by abundant high-Mg garnets (Prp > 30 mol%), thus, they contain relatively high percentages of Type A garnets (Fig. 10e). Furthermore, the analyzed garnet grains are scattered in the ternary diagram, and show variable Prp and Grs contents (Fig. 10d) with maximums of 43.3 mol% and 37.4 mol%, respectively. The detrital garnets of Sample B1-05, which are dominated by Type B garnet, are near the Type B apex in the Type A-B-C ternary diagram (Fig. 10e). The detrital garnets of Samples LLH-30, LLH-47 and LLH-58 are dominated by Type B garnet, and show relatively high Mn contents. Similarly, the chemical data of these garnet grains are scattered and display variable Prp and Grs contents (Fig. 10d).

6.2. Detrital tourmaline chemistry

Tourmaline is a complex borosilicate mineral with a large amount of potential element substitutions. The main chemical variations are commonly expressed by Mg, Fe, Ca and Al substitutions (Henry and Guidotti, 1985). Tourmaline is a common accessory mineral that is found in many rock types. It occurs in many clastic sedimentary rocks as a stable heavy mineral; and can be found in metamorphic rocks with a wide variety of types, granitoid intrusive rocks and their associated pegmatites, aplites and hydrothermal alteration zones (Deer et al., 1992).

Henry and Guidotti (1985) proposed using Al-Al50Fe(tot)50-Al50Mg50 and Ca-Fe(tot)-Mg ternary diagrams to identify different tourmaline-bearing parent rock types. Several distinct regions can be defined for tourmalines from different rock types (Fig. 11). Calculations and classifications by the CLASTOUR program (Yavuz et al., 2002) reveal that most of the tourmalines belong to alkali group. The results show that the main chemical variation is the substitution between Fe and Mg. Representative chemical compositions of these detrital tourmalines are shown in Table A.4 (in Appendix A online). Fig. 11 displays the Al–Fe(tot)–Mg ternary plot of detrital tourmalines for each sample.

Detrital tourmalines of Samples B1-01 and X9-01 are relatively scattered in the ternary diagram (Fig. 11). They mainly fall in Field 2, followed by Fields 4 and 5, whereas minor grains fall in Fields 3 and 6. However, the detrital tourmalines of Samples YCG-08 and YCG-17 have distinctive compositions that clearly distinguish them from the detrital tourmalines of Samples B1-01 and X9-01 (Fig. 11). The tourmalines primarily fall in Fields 4 and 5, whereas the tourmalines in Fields 2 and 6 are scarce, revealing relatively centralized distribution.

7. Discussion

7.1. Methodological evaluation

To accomplish the provenance study, we present an integrated study with the use of detrital framework grain composition, heavy mineral and mineral chemical data. No individual dataset can provide the spatial and temporal variation of provenance. The design can be explained as follows.

First, the framework grain composition data were used to discriminate the provenance settings (Fig. 4). However, both raw data and statistical analysis results indicate similar spatial illustrations (Figs. 4–6). Almost all locations (except No. 4 Lenghu) exhibit similar mean framework grain compositions in log-ratio ellipsoid confidence regions (Fig. 6). Because the groups cannot be significantly discriminated, other types of data are required.

Heavy mineral data were advocated. Based on the results of heavy mineral assemblages, ratios and log-ratio confidence regions in ternary diagrams (Figs. 7–9), two types of heavy minerals, which differ significantly from each other, can be distinguished. The first type includes the heavy minerals of Mahai, Beilingqiu, Nanbaxian and No. 7 Lenghu areas; whereas the second type includes the heavy minerals of No. 5 Lenghu, Yingchaogou, Jielusu and Quandonggou areas. However, the results of Eboliang, No. 3 Lenghu, No. 4 Lenghu, as well as the results of Lulehe outcrop are uncertain. Are the data of Eboliang, No. 3 Lenghu and No. 4 Lenghu discriminated from the preceding two types because

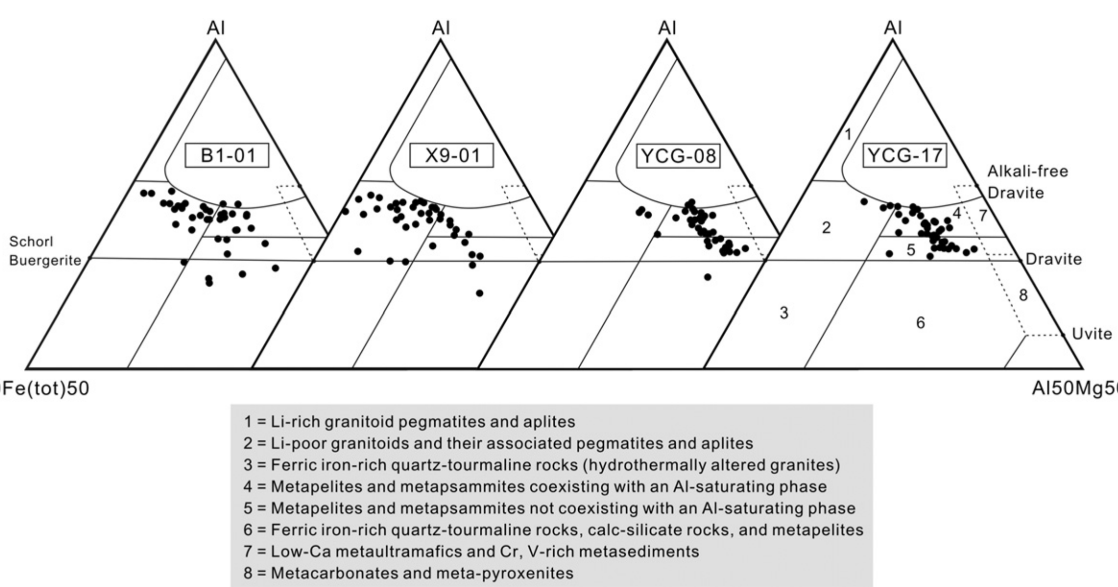

Fig. 11. Detrital tourmaline chemistry of selected sandstones. The provenance-discrimination ternary diagrams (in molecular proportions) were devised by Henry and Guidotti (1985). For representative data, see Table A.4 (in Appendix A online).

they are scattered? Should the Lulehe outcrop be added to the first type because it is adjacent to Mahai?

Mineral chemical data of detrital garnet and tourmaline were obtained to resolve these uncertainties. Our results indicate that Samples K2-03 (No. 3 Lenghu) and S81-01 (No. 4 Lenghu) differ from other samples, implying a different source (Fig. 10d). The detrital garnet data of three samples of Lulehe outcrop are scattered, which is similar to the detrital garnet data of Mahai, Beilingqiu, Nanbaxian and No. 7 Lenghu. However, the chemical compositions of detrital garnets reveal a slight temporal variation, whereas the data of framework grain composition and heavy mineral analysis differ among various formations. In addition, individual mineral chemical data only demonstrate the derivation of this single analyzed mineral species. The data of framework grain composition and heavy minerals are considered together for the parent rocks of sandstones. Therefore, integration of these three types of data was proposed to provide a provenance interpretation.

7.2. Spatial variation of provenance and depositional areas

Overall, the Tertiary sediments of the northern Qaidam basin seem to have an overwhelming derivation from an orogen source (Fig. 4a). To analyze the spatial variation of provenance, samples were grouped based on locations. Three types of depositional areas can be distinguished based on the differences of the three types of data.

7.2.1. Depositional area A

Sandstones from Mahai, Beilingqiu, Nanbaxian and No.7 Lenghu exhibit relatively high textural maturity (e.g., Fig. 6A, E) and contain relatively abundant quartz. Heavy minerals in these sandstones are characterized by high garnet (Fig. 7a) and ZTR mineral abundances (except hematite), high ZTR and stability indexes, low GZi, RuZi and Eti values (Fig. 9). Detrital garnets of these sandstones are dominated by Type B garnets with a certain proportion of Type A garnets due to the relatively abundant high-Mg garnets (Fig. 10d). The compositions of analyzed garnet grains are scattered (Fig. 10d), which implies various parent rock types. These garnets are most likely derived from low- to medium-grade metasedimentary rocks and subordinate high-grade granulite-facies metasediments (Morton et al., 2004, 2005), or from intermediate-acidic igneous rocks (e.g., high-temperature granites and their associated pegmatites and aplites) from deep in the crust (Mange and Morton, 2007). Detrital tourmalines in sandstones from Beilingqiu and Nanbaxian are composed of dravites and schorls (Fig. 9, Table 1), indicating the two types of derivations, i.e., granites and metasediments (Henry and Guidotti, 1985). All analysis results suggest that Mahai, Beilingqiu, Nanbaxian and No.7 Lenghu have similar source rocks. Hence, they are located in the same depositional area (Depositional area A).

Heavy minerals in sandstones from the Lulehe outcrop also exhibit high garnet abundances (high GZi values), moderate ZTR, high stability indexes, and low RuZi and Eti values. Although log-ratio ellipsoidal confidence fields of heavy mineral assemblages of these sandstones differ from the log-ratio ellipsoidal confidence fields of Mahai, Beilingqiu and Nanbaxian in the ternary diagrams (Fig. 8), the compositions of detrital garnets are scattered and similar to the garnet compositions of the above four areas (Fig. 10d). Hence, we suggest that the Lulehe area can be added to Depositional area A, because it is spatially close to

Table 1
The Integration of the results of framework grain point counting, heavy mineral analysis and mineral chemistry for sandstone samples of each location.

Location	Framework grain	Heavy mineral						Mineral chemistry		Depositional areas and provenance interpretations
	Qm-F-Lt	heavy mineral assemblages	ZTR index	stability index	GZi	RuZi	ETi	Detrital garnet	Detrital tourmaline	
LLH Outcrop	–	grt + hem + ilm + tur + ep	6–18(10)	1.6–40.9(9.4)	86–100(96)	0–38(19)	33–95(74)	10.8:77.5:11.7	–	Depositional area A. The sediments were derived from various metasedimentary rocks and intermediate-acidic igneous rocks, or with subordinate high-grade basic metamorphic rocks. And the metamorphic source rocks source increased over time.
Mahai	51:15:34	grt + hem + ilm + zrn + leu	15–53(32)	1.6–22.3(6.6)	7–83(56)	13–26(18)	0–89(37)	22.5:60:17.5	–	
Beilingqiu	55:15:30	hem + grt + zrn + leu + ilm	31–35(34)	3.8–12.5(9.1)	43–76(61)	9–25(16)	46–100(79)	10:85:5	45 (D): 55 (S)	
Nanbaxian	54:14:32	hem + grt + zrn + leu + Ap	20–50(36)	2.6–28.5(11.7)	17–92(50)	6–19(11)	0–92(22)	22.5:65:12.5	27.5 (D): 72.5 (S)	
No. 7 Lenghu	46:25:29	hem + zrn + grt + leu + Ap	56	16.9	32	8	17	25:67.5:7.5	–	
Pingtai	–	ilm + grt + ep + hem + zrn	10–30(20)	1.1–4.2(2.6)	69–87(78)	11–24(18)	48–88(68)	–	–	Depositional area B. The sediments have a nearby source and display a dominate derivation of low-to-medium grade metasedimentary source rocks.
No. 5 Lenghu	47:14:38	ep + grt + ilm + hem + ttn	2–19(9)	0.3–2.2(1.4)	71–98(87)	6–50(26)	69–98(79)	12.5:85:2.5	–	
YCG Outcrop	47:16:36	ep + hem + grt + hbl + ilm	1–14(6)	0.1–1.8(0.7)	65–97(88)	10–50(25)	78–97(90)	3:76:21	87.5 (D): 10 (S): 2.5 (O)	
QDG Outcrop	–	ep + hem + grt + hbl + mag	1–22(12)	0.1–1.5(0.7)	65–97(75)	11–55(27)	69–100(84)	–	–	
JLS Outcrop	–	hem + ep + grt + ttn + mag	5–10(8)	0.5–1.1(0.8)	86–91(89)	24–33(27)	90–96(94)	2.5:97.5:0	–	
No. 3 Lenghu	45:33:22	hem + grt + ttn + ep + ilm	9–13(11)	2.2–5.8(4.0)	55–86(71)	2–8(5)	29–35(32)	10:90:0	–	Depositional area C. The sediments show a main derivation of igneous source rocks with subordinate metamorphic source rocks. The igneous source rocks increased over time.
No. 4 Lenghu	43:23:34	hem++ilm + grt + leu + ep	8–43(24)	2.9–39.7(11.9)	52–83(64)	7–31(16)	41–100(76)	2.5:95:2.5	–	
Eboliang	55:17:28	hem + grt + zrn + leu + ep	6–45(26)	2.5–8.9(5.7)	46–96(71)	20–29(25)	0–100(50)	–	–	

For location see Fig. 1b, and for abbreviations of framework grains, heavy minerals and ratios see Table A.2 and Table A.3 (in Appendix A online).
Qm-F-Lt for each area is shown in average values. Heavy mineral assemblages are shown as five species heavy minerals in the order of abundances, and the indexes and ratios are shown as minimums and maximums with the average in brackets behind. Need to note that the heavy mineral analysis result of No. 7 Lenghu is from only one sample. The results of garnet chemistry are shown as the average ratios of the abundances of Type A, Type B and Type C garnets, respectively. The results of tourmaline chemistry are shown as the ratios of the abundances of different kinds of tourmalines calculated by CLASTOUR program (Yavuz et al., 2002), such as dravite (D) and schorl (S), in this column, "others" (O) includes uvite and foitite, which are infrequent in the samples from the northern Qaidam basin.

Mahai. Furthermore, the ZTR index of these five areas displays in the order of No.7 Lenghu > Nanbaxian > Beilingqiu > Mahai > Lulehe outcrop, with averages of 56, 36, 34, 32 and 10 respectively (Table 1). Stratigraphic correlation (Fig. 12) indicates that No. 7 Lenghu contains the thickest strata (e.g., Xia Ganchaigou Formation). Paleocurrent measurements demonstrate strong unimodal paleocurrent toward the southwest in the Lulehe area (Zhuang et al., 2011). Therefore, it is inferred that No. 7 Lenghu is in close proximity to the lake area, whereas the Lulehe outcrop is in close proximity to the source area (Fig. 13).

The provenance for Depositional area A is mixed and of long-distance. The parent rocks are most likely dominated by various grades of metasedimentary rocks and intermediate-acidic igneous rocks. Because the North Qaidam and South Qilian terranes are mainly composed of schists, gneisses and amphibolites of the Proterozoic Dakendaban Group (Zhang et al., 2009a; Mattinson et al., 2009; Menold et al., 2009; Wang et al., 2009) and Early Paleozoic granites and granodiorites (Gehrels et al., 2003), they are most likely the sediment sources for Depositional area A.

7.2.2. Depositional area B

Sandstones from No. 5 Lenghu and Yingchaogou exhibit relatively low textural maturity (e.g., Fig. 6C) and high metamorphic lithic fragment abundances (Fig. 3, Table 1). Heavy minerals are primarily composed of epidote and garnet (Fig. 7b), with subordinate ilmenite. The samples display low ZTR and stability indexes and relatively high GZi, RuZi and Eti values (Fig. 9). Detrital garnets are dominated by Type B garnets (Fig. 10d), indicating a predominant source of low- to medium-grade metasedimentary rocks. The small proportion of Type C garnets (e.g., Sample YCG-02 and YCG-08) are derived from high-grade metabasic rocks (Morton et al., 2004, 2005). Detrital tourmalines of sandstones from the Yingchaogou outcrop are mainly composed of dravites (Fig. 11; Table 1) and have the dominated derivations of metasediments, including Al-rich and Al-poor types (Henry and Guidotti, 1985). Sandstone samples of the Pingtai, Quandonggou and Jielusu areas also exhibit similar heavy mineral characteristics (Table 1). Additionally, sandstones of these locations display distinctive confidence regions of heavy mineral assemblage than sandstones of Depositional area A (Fig. 8). All these results imply an obviously different depositional area, which is defined as Depositional area B. Similarly, according to the stratigraphic correlation (Fig. 12), ZTR and stability indexes (Table 1) and textures, a relatively close provenance in the direction from Yingchaogou to No.5 Lenghu (Fig. 13) is suggested.

Integration of these three types of data indicates that the provenance of the sediments in Depositional area B is practically simplex. The dominating parent rock types are metamorphic rocks, including low- to medium-grade metasedimentary rocks and high-grade metabasic rocks; thus, the sediment source can be constrained within the North Qaidam and South Qilian metamorphic belts, such as schists and gneisses of the Proterozoic Dakendaban Group, and basic metamorphic rocks of the lower Paleozoic Tanjianshan Group (Gehrels et al., 2003; Song et al., 2003a,b, 2005, 2006; Yang et al., 2006; Song et al., 2007a,b).

7.2.3. Depositional area C

Sandstones of No. 3 Lenghu, No. 4 Lenghu and Eboliang contain relatively high abundances of feldspar (Table 1; Figs. 4 and 5), and the log-ratio confidence region of No. 4 Lenghu in the QFL ternary diagram differs from the locations of Depositional areas A and B (Fig. 6). Heavy minerals are dominated by garnet and ilmenite, with subordinate ZTR minerals and leucoxene. The samples display relatively moderate ZTR and stability indexes and GZi, RuZi and Eti values (Table 1). However, the heavy mineral data with small sample sizes are scattered (Fig. 9), i.e., with larger uncertainties, which result in the much larger confidence ellipsoids in the ternary diagram (Fig. 8). The detrital garnet chemical data indicate the dominance of Type B garnets with very high Fe + Mn contents (Samples K2-03 and S81-01, Fig. 10d), which suggests a major potential derivation of low- and medium-temperature granites (Mange and Morton, 2007).

Integration of these data suggests that No. 3 Lenghu, No. 4 Lenghu and Eboliang compose Depositional area C in which igneous rocks (including intermediate-acidic rocks and basic rocks) are the main source rocks for sediments. Metamorphic parent rocks (e.g., schists and gneisses) also serve as secondary source rocks. Because the southern flanks of the Altun Mountains consist of Paleozoic and Mesozoic granites, diorites, metamorphic rocks and Jurassic sedimentary rocks (Gehrels et al., 2003; Yang et al., 2006; Mattinson et al., 2007), the Altun Mountains are most likely to be the dominant sediment sources for Depositional area C. While the Qilian Mountains most likely serve as the subordinate sources. Therefore, it is inferred that sediments of Depositional area C were constrained by a mixed provenance of the Altun and Qilian Mountains.

7.3. Stratigraphic variation of provenance for three depositional areas

Samples were grouped by formations for each depositional area. The stratigraphic variations of sandstone average detrital compositions and log-ratio confidence ellipsoids are illustrated in Figs. 14 and 15. The temporal compositional trends of Lulehe and Yingchaogou are shown in Figs. 16 and 17 as the representative profiles of Depositional area A and Depositional area B, respectively. The details and corresponding provenance interpretations are described in the next sections.

7.3.1. Depositional area A

The data of framework grain compositions reveal decreasing quartz abundance and increasing lithic fragment abundance through

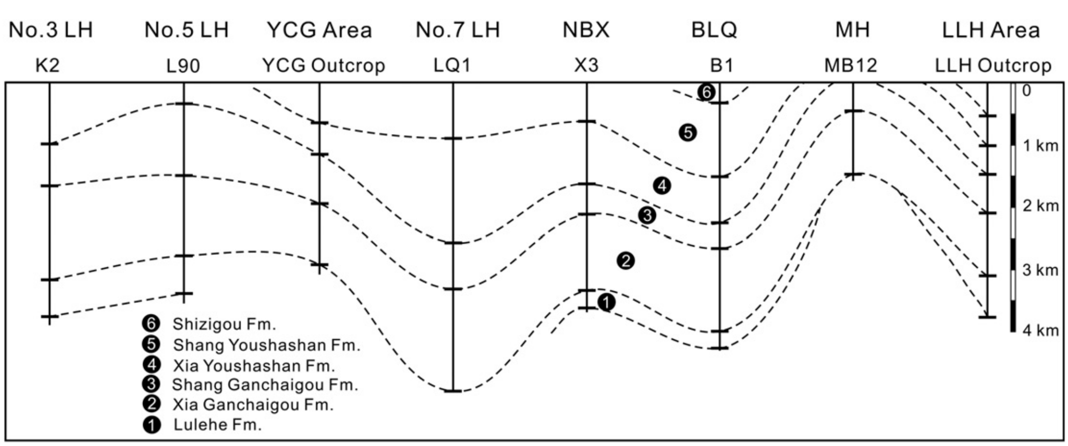

Fig. 12. Schematic diagram of stratigraphic correlation of selected drilling wells and outcrops in the northern Qaidam basin. Well L90 is located in No. 5 Lenghu, which is near Well L87. For abbreviations see Fig. 1.

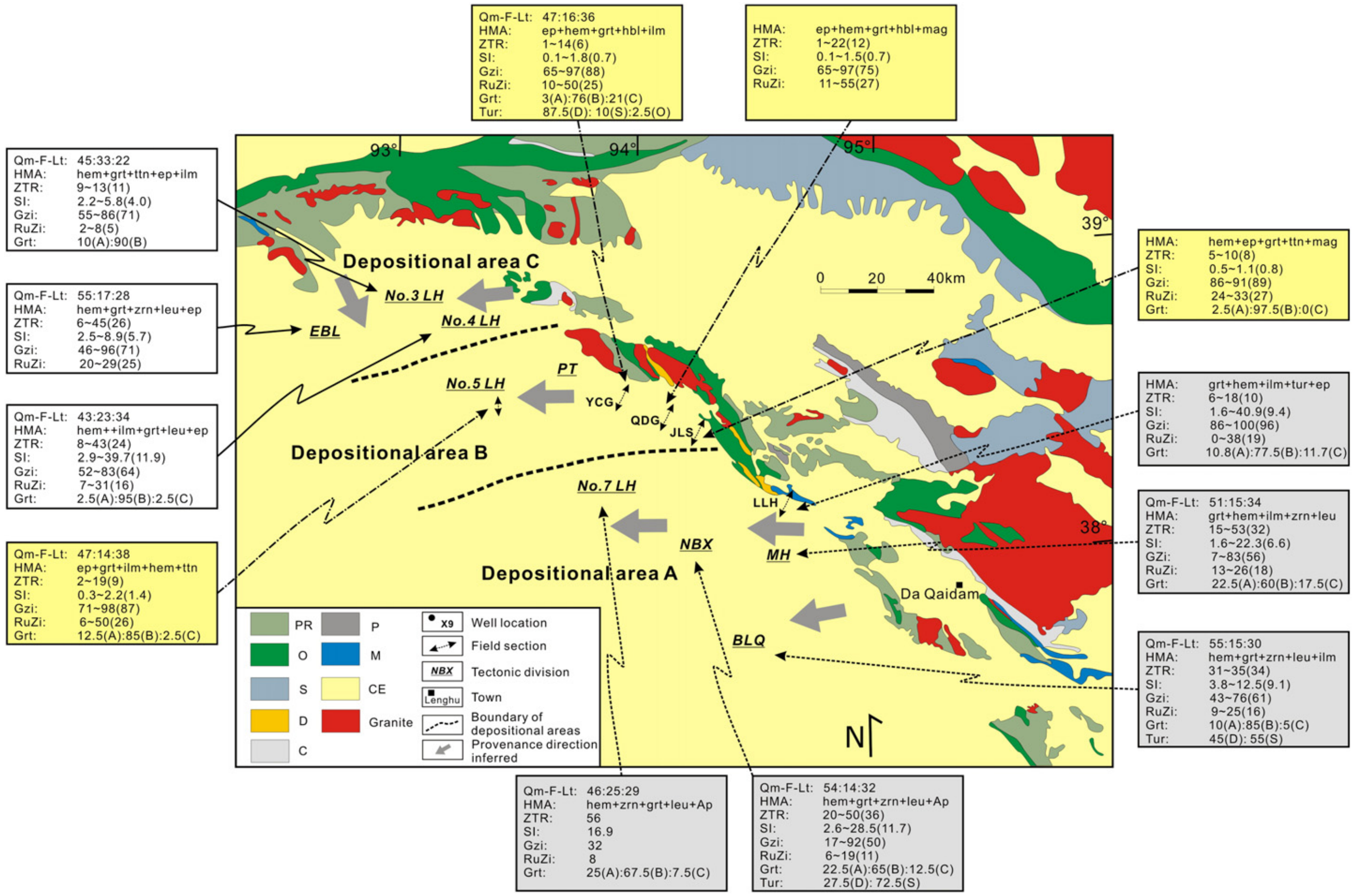

Fig. 13. Discrimination of Tertiary depositional areas in the northern Qaidam basin. The potential provenance directions (gray arrows) were inferred. HAM: heavy mineral analysis; PR: Proterozoic Dakendaban Group, mainly composed of schists, gneisses and amphibolites with subordinate marbles (Mattinson et al., 2009; Menold et al., 2009); O: Ordovician, Tanjianshan Group, phyllites, schists, marbles, sandstones, limestones and subordinate igneous rocks (Gehrels et al., 2003); S: Silurian, silicolites; D: Devonian, sandstones and igneous rocks; C: Carboniferous, limestones, sandstones and subordinate schists; P: Permian, limestones; M: Jurassic and Cretaceous, sandstones; CE: Cainozoic.

the stratigraphic age in Depositional area A (Fig. 14a). Heavy mineral data indicate that the metamorphic source minerals (e.g., epidote and garnet) exhibited increasing trends (Fig. 15a, d). The heavy mineral temporal variation of sandstones of the Lulehe outcrop indicates that the abundances of ilmenite, hornblende and pyroxene are relatively high for the samples of the Xia Ganchaigou and Shang Ganchaigou Formations, whereas garnet and epidote are distinctly enriched in the samples of upper formations (Fig. 16). All results imply an increasing metamorphic source and a decreasing igneous source for Depositional area A.

7.3.2. Depositional area B

The sandstones of Xia Ganchaigou Formation display high abundances of quartz; conversely, the sandstones of the upper formations contain relatively low abundances of quartz and high abundances of lithic fragment (Fig. 14b). Heavy mineral data indicate a significant variation between the Lulehe and Xia Ganchaigou Formtions (Fig. 15b), showing remarkably decreasing minerals of igneous source; the heavy mineral assemblages vary slightly above the Xia Ganchaigou Formation, displaying increasing garnets and epidotes and decreasing ZTR minerals (Fig. 15b, e). Similar variation trends can be found in the Yingchaogou outcrop (Fig. 17). The stratigraphic variation trends of detrital components of Depositional area B are similar to the stratigraphic trends of Depositional area A, which implies increasing metamorphic provenance and decreasing igneous provenance. Additionally, low abundances of Type C garnet (Fig. 17) in the upper formations suggest a reduction of high-grade basic metamorphic parent rocks.

7.3.3. Depositional area C

In this area, the sandstones are characterized by increasing amounts of feldspar and igneous- source heavy minerals (e.g., ilmenite and ZTR minerals) from the Lulehe Formation to the Shang Ganchaigou Formation (Figs. 14c and 15c, f), which implies an increasing igneous source over time. Furthermore, the sandstone of Shang Ganchaigou Formation (e.g., Sample K2-03) seemingly contains more abundant high-Fe + Mn garnets (plot near the Alm + Sps apex, i.e., Fe + Mn > 90%) than the Lulehe Formation (e.g., Sample S81-01), indicating an increase of detrital garnets of granite derivation (Fig. 10). Hence, it is inferred that the igneous rocks, especially the intermediate-acid igneous rocks, were increasingly exhumated and denudated as the parent rocks for Depositional area C.

7.4. Tectonic implications

The clastic sedimentation of Qaidam basin has been constrained by the regional tectonic events occurring in the northeastern Tibetan Plateau. Zhuang et al. (2011) investigated eleven Cenozoic sedimentary sections from the Qaidam basin, Hexi Corridor and Subei basin, and proposed four phases of tectonic history of the northern Tibetan Plateau. However, the Cenozoic succession of the northern Qaidam basin records three phases of these tectonic events (Zhuang et al., 2011; Jian and Guan, in review).

The coarse-grained clastic sediments of the Lulehe Formation are considered as the synorogenic sedimentary records of a strong differentiation between the Qaidam basin and surrounding mountains, which

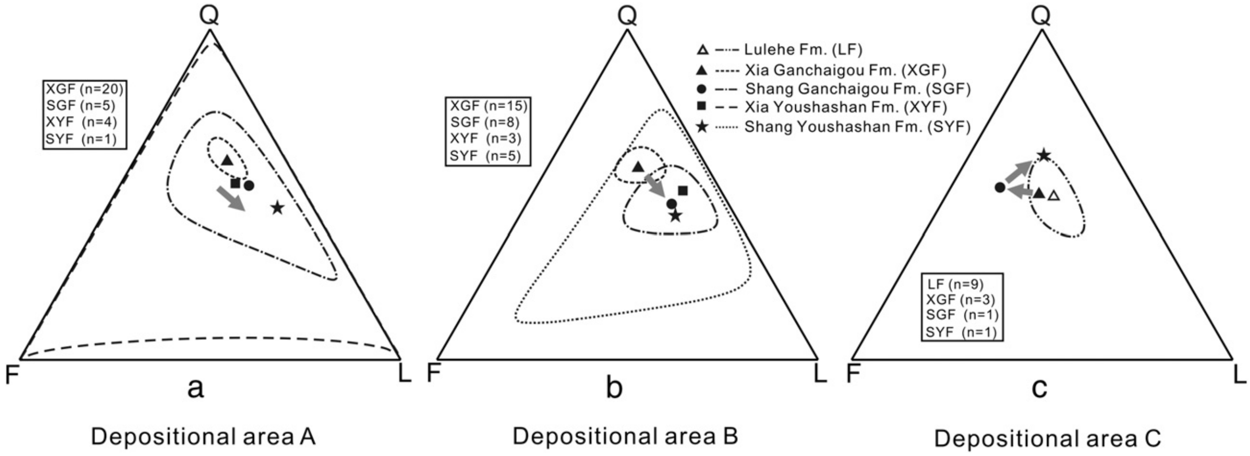

Fig. 14. QFL ternary diagrams displaying the stratigraphical variations of detrital framework grain compositions of sandstones in three Depositional areas. Geometric means and 95% confidence ellipsoids ($n > 3$) calculated using the log-ratio method (Weltje, 2002). Samples are grouped by formations. The gray arrows depict the variation trends.

may be the far-field effects of the India–Eurasia collision (Zhuang et al., 2011; Jian and Guan, in review). In this stage, the North Qaidam and South Qilian terranes, which primarily provided clastic materials for Depositional areas A and B, were mainly composed of igneous rocks and metamorphic rocks. Our inference differs slightly from the results of the previous study of conglomerate clast components (Zhuang et al., 2011), which indicated considerable carbonate contents. However, the provenance region of the Altun Mountains, which mainly provided materials for Depositional area C, consisted of dominant igneous rocks and subordinate metamorphic rock. The uplift of Altun Mountains remains controversial (Meng et al., 2001; Sobel et al., 2001; Yin et al., 2002). Previous studies suggested that the Altun Mountains experienced a multiple stages uplift history (Sobel et al., 2001; Ritts et al., 2008) with initial uplift since at least the early Oligocene or possibly late Eocene (Yin et al., 2002). Recently, we conclude that an orogeny and tectonic uplift event of the entire basin scale occurred during the early–middle Eocene (Jian and Guan, in review), which resulted in the unroofing of the Altun Mountains region and the exposure of igneous parent rocks. They were subsequently denudated and rapidly flattened after initial tectonic uplift.

The main fine-grained sediments from the Xiaganchaigou Formation to the Xia Youshashan Formation formed in response to the relatively quiet tectonic background of the northern Qaidam basin (Jian and

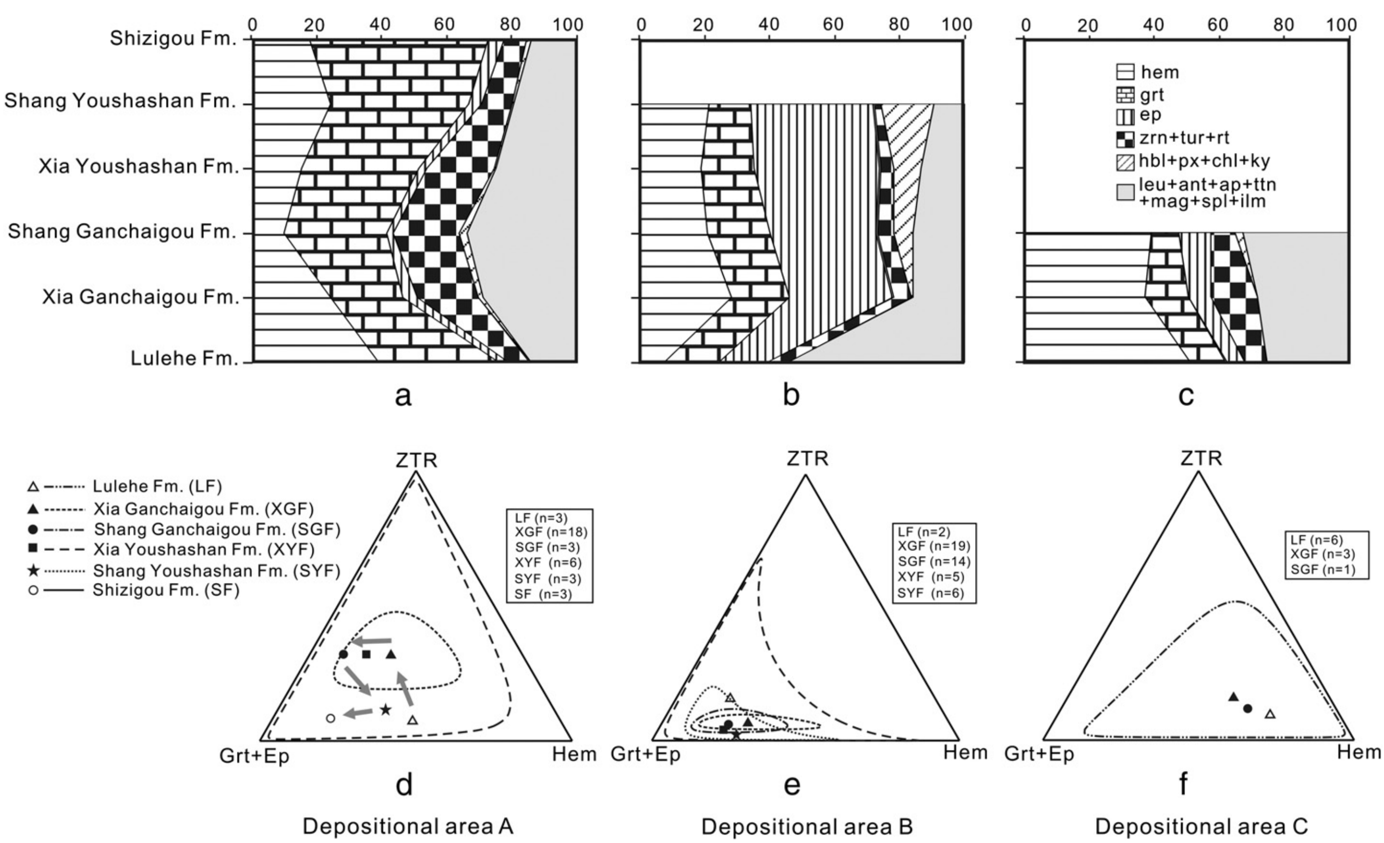

Fig. 15. Area diagrams and Ternary diagrams displaying the stratigraphical variations of heavy minerals of sandstones in three Depositional areas. Geometric means and 95% confidence ellipsoids ($n > 3$) in (d), (e) and (f) calculated by using the log-ratio method (Weltje, 2002). Samples are grouped by formations. The gray arrows indicate the variation trends of the heavy minerals. For data and abbreviations see Table A.3 (in Appendix A online).

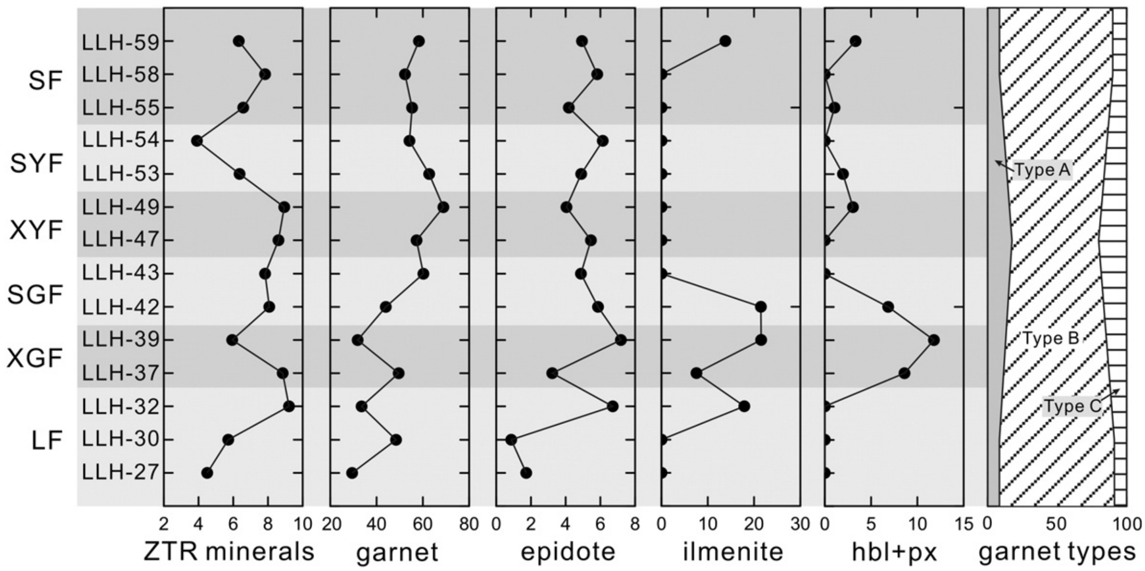

Fig. 16. Temporal variations of heavy minerals and detrital garnet types of sandstones of the Lulehe outcrop.

Guan, in review). This finding is also supported by the contents of stable heavy minerals and ZTR and stability indexes (e.g., Figs. 15 and 16). The relatively calm tectonic setting resulted in remarkable changes in the sedimentary facies and depositional system (Zhuang et al., 2011; Jian and Guan, in review). Variation of the detrital components of sandstones indicates variation in the source rock distributions compared with the first stage (Figs. 14–17). The sources of Depositional areas A and B contain an increasing metamorphic rocks (distinctly for area B), which implies an increasing exhumation and denudation of North Qaidam and South Qilian metamorphic belts. The source of Depositional area C contains increasing amounts of igneous rocks, which is most likely in response to another uplift event of the Altun Mountains (Sobel et al., 2001; Ritts et al., 2008).

The coarse-grained clastic sediments of the Shang Youshashan Formation to the Shizigou Formation may be related to the intense basin-range differentiation caused by the crustal shortening and rapid tectonic uplift of the northern Tibetan Plateau (Harrison et al., 1992; Molnar et al., 1993). It is suggested that the source rock distributions in this stage nearly inherited the character of the second stage, based on detrital components of sandstones in Depositional areas A and B. The increasing abundances of garnet and epidote (Figs. 15 and 16) and the dominant metamorphic gravels in conglomerates (Zhuang et al., 2011; Jian and Guan, in review) favor the significance of metamorphic parent rocks. Therefore, we infer that the North Qaidam and South Qilian metamorphic belts have been widely exposed since this stage.

8. Conclusions

From the use of sandstone framework petrography, heavy mineral analysis and mineral chemistry, we have accomplished the provenance analysis of the Tertiary sandstone in the northern Qaidam basin. Based on integration of these three types of data, provenance interpretations and spatial and stratigraphic variations were provided. However, none of the individual datasets were able to solve them.

The Dickinson model (Dickinson, 1985) analysis of framework grain compositions suggests that the Tertiary sandstones of the northern Qaidam basin have an overwhelming derivation from an orogen source, including quartzose, transitional recycled orogenic sources, and a small proportion of mixed sources. The means and corresponding log-ratio confidence regions of framework grain compositions exhibit only a slight spatial variation.

Three depositional areas were spatially distinguished and their provenances were interpreted by combining three types of data. Depositional area A is comprised of Lulehe outcrop, Mahai, Beilingqiu, Nanbaxian and No. 7 Lenghu. The detrital clastics experienced relatively long-distance transport. A variety of detrital components (including heavy mineral

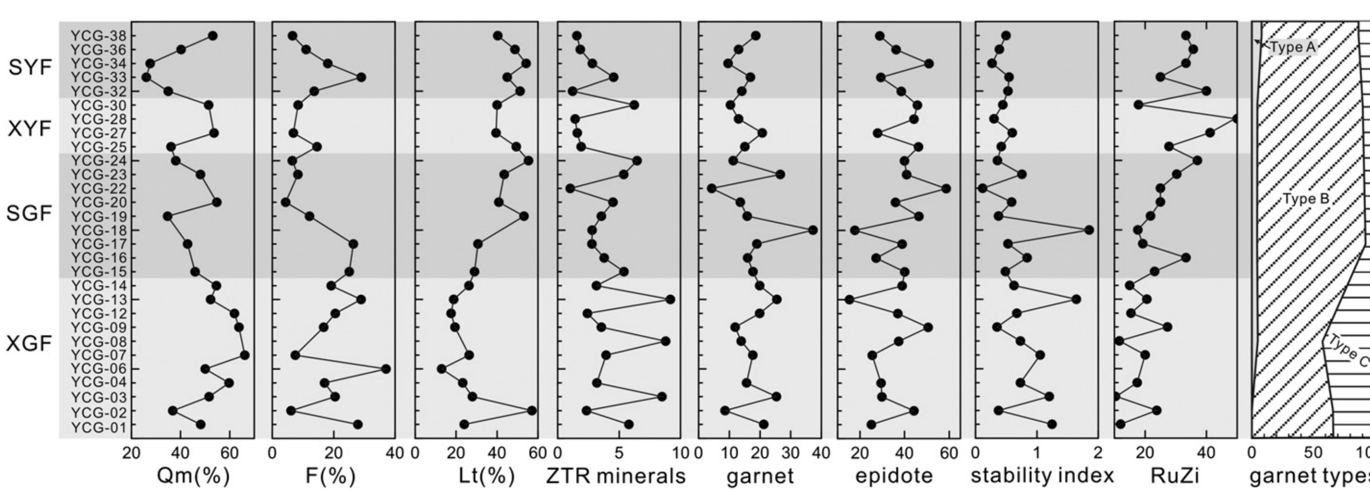

Fig. 17. Temporal variations of framework grain components, heavy minerals, heavy mineral indexes and ratios and garnet types of sandstones of the Yingchaogou outcrop.

assemblages and detrital garnet and tourmaline type data) suggest multi-type source rocks, which are most likely dominated by various grades of metasedimentary rocks and intermediate-acidic igneous rocks. Depositional area B consists of Yingchaigou, Quandonggou, Jielusu outcrops, Pingtai and No.5 Lenghu. The data of detrital components reveal that this area has an adjacent source region in which low- to medium-grade metasedimentary rocks serve as the predominant parent rocks. The sediment source of these two depositional areas can be constrained within the North Qaidam and South Qilian belts of the Qilian Mountains. However, the third area, i.e., Depositional area C, which comprises No. 3 Lenghu, No. 4 Lenghu and Eboliang, differ significantly from Depositional areas A and B. The source rocks are composed by dominant igneous rocks with subordinate metamorphic rocks. Thus, the Altun and Qilian Mountains are most likely regarded as potential source regions, and yet the Altun Mountains provide more materials for this depositional area.

Stratigraphically, the vertical variations of detrital components of sandstones and corresponding provenance interpretations provide additional data regarding tectonic evolutions of the northern Tibetan Plateau. It is proposed that the source of Depositional areas A and B presented a variation trend of increasing abundances of metamorphic rocks, which suggest the increasing exhumation and unroofing of two metamorphic belts during the tectonic uplift of the Qilian Mountains. However, the source of Depostional area C revealed an increasing abundance of igneous rocks, which implies an increase in clastic sources in the Altun Mountains in response to multi-stage uplift events of those mountains.

Supplementary data to this article can be found online at http://dx.doi.org/10.1016/j.sedgeo.2013.03.010.

Acknowledgments

This research was supported by PetroChina Qinghai Oilfield Company. We would like to thank Qiang Wei and Shibiao Deng of Peking University for participating in the study, Guiming Shu of Peking University for the assistance in EPMA analyses, and Prof. Shuguang Song and Jinxue Du of Peking University for their helpful suggestions. We are grateful to Huan Cui of the University of Maryland and Rui Wang of the University of Alberta for their significant efforts in improving the English grammar of the manuscript. We also appreciate the two anonymous reviewers, the Language Editor and the Editor-in-Chief Gert Jan Weltje and Brian Jones for their helpful and constructive comments on the early version of this manuscript.

References

Aitchison, J., 1986. The Statistical Analysis of Compositional Data. Chapman and Hall, London.
Allen, J.L., Johnson, C.L., 2010. Facies control on sandstone composition (and influence of statistical methods on interpretations) in the John Henry Member, Straight Cliffs Formation, Southern Utah, USA. Sedimentary Geology 230, 60–76.
Comas-Cufí, M., Thió-Henestrosa, S., 2011. CoDaPack 2.0: a stand-alone, multi-platform compositional software. In: Egozcue, J.J., Tolosana-Delgado, R., Ortego, M.I. (Eds.), CoDaWork'11: 4th International Workshop on Compositional Data Analysis (Sant Feliu de Guíxols). International Center for Numerical Methods in Engineering, Barcelona, Spain.
Deer, W.A., Howie, R.A., Zussman, J., 1992. An Introduction to Rock-forming Minerals. Longman Group Limited, Hong Kong (696 pp.).
Dickinson, W.R., 1985. Interpreting provenance relations from detrital modes of sandstones. In: Zuffa, G.G. (Ed.), Provenance of Arenites. Reidel, Dordrecht (333-336 pp.).
Dickinson, W.R., Suczek, C.A., 1979. Plate tectonics and sandstone compositions. AAPG Bulletin 63, 2164–2182.
Egozcue, J.J., Pawlowsky-Glahn, V., Mateu-Figueras, G., Barceló-Vidal, C., 2003. Isometric log ratio transformations for compositional data analysis. Mathematical Geology 35, 279–300.
Garzanti, E., Vezzoli, G., Andò, S., Paparella, P., Clift, P.D., 2005. Petrology of Indus River sands: a key to interpret erosion history of the Western Himalayan syntaxis. Earth and Planetary Science Letters 229, 287–302.
Garzanti, E., Andò, S., Vezzoli, G., Ali Abdel Megid, A., El Kammar, A., 2006. Petrology of Nile River sands (Ethiopia and Sudan): sediment budgets and erosion patterns. Earth and Planetary Science Letters 252, 327–341.
Gehrels, G.E., Yin, A., Wang, X.F., 2003. Magmatic history of the northeastern Tibetan Plateau. Journal of Geophysical Research 108 (B9), 2423.
Hallsworth, C.R., Chisholm, J.I., 2008. Provenance of late Carboniferous sandstones in the Pennine Basin (UK) from combined heavy mineral, garnet geochemistry and palaeocurrent studies. Sedimentary Geology 203, 196–212.
Hallsworth, C.R., Morton, A.C., Claoué-Long, J., Fanning, C.M., 2000. Carboniferous sand provenance in the Pennine Basin, UK: constraints from heavy mineral and detrital zircon age data. Sedimentary Geology 137, 147–185.
Hanson, A.D., Ritts, B.D., Zinniker, D., Moldowan, J.M., Biffi, U., 2001. Upper Oligocene lacustrine source rocks and petroleum systems of the northern Qaidam basin, northwest China. AAPG Bulletin 85, 601–619.
Harrison, T.M., Copeland, P., Kidd, W.S.F., Yin, A., 1992. Raising Tibet. Science 255, 1663–1670.
Henry, D.J., Guidotti, C.V., 1985. Tourmaline as a petrogenetic indicator mineral: an example from the staurolite-grade metapelites of NW Maine. American Mineralogist 70, 1–15.
Ingersoll, R.V., Eastmond, D.L., 2007. Composition of modern sand from the Sierra Nevada, California, U.S.A.: implications for actualistic petrofacies on continental margin magmatic arcs. Journal of Sedimentary Research 77, 784–796.
Ingersoll, R.V., Suczek, C.A., 1979. Petrology and provenance of Neogene sand from Nicobar and Bengal fans, DSDP sites 211 and 218. Journal of Sedimentary Petrology 49, 1217–1228.
Ingersoll, R.V., Bullard, T.F., Ford, R.L., Grimm, J.P., Pickle, J.D., Sares, S.W., 1984. The effect of grain size on detrital modes: a test of the Gazzi–Dickinson point-counting method. Journal of Sedimentary Petrology 54, 103–116.
Jian, X., Guan, P., in review. The sedimentary record in Qaidam basin and its implications for tectonic and climatic evolution of the northern Tibetan Plateau. Chinese Journal of Geology (in Chinese with English abstract).
Li, Z., Song, W., Peng, S., Wang, D., Zhang, Z., 2004. Mesozoic–Cenozoic tectonic relationships between the Kuqa subbasin and Tian Shan, northwest China: constraints from depositional records. Sedimentary Geology 172, 223–249.
Liu, Z., Wang, Y., Ye, C., Li, X., Li, Q., 1998. Magnetostratigraphy and sedimentologically derived geochronology of the Quaternary lacustrine deposits of a 3000 m thick sequence in the central Qaidam basin, western China. Palaeogeography, Palaeoclimatology, Palaeoecology 140, 459–473.
Liu, Y.-J., Neubauer, F., Genser, J., Takasu, A., Ge, X.-H., Handler, R., 2006. 40Ar/39Ar ages of blueschist facies pelitic schists from Qingshuigou in the Northern Qilian Mountains, western China. The Island Arc 15, 187–198.
Mange, M.A., Maurer, H.F.W., 1992. Heavy Minerals in Color. Chapman and Hall, London.
Mange, M.A., Morton, A.C., 2007. Geochemistry of heavy minerals. In: Mange, M.A., Wright, D.T. (Eds.), Heavy Minerals In Use: Developments in Sedimentology, 58, pp. 345–391.
Mattinson, C.G., Wooden, J.L., Liou, J.G., Bird, D.K., Wu, C.L., 2006. Age and duration of eclogite-facies metamorphism, North Qaidam HP/UHP terrane, western China. American Journal of Science 306, 683–711.
Mattinson, C.G., Menold, C.A., Zhang, J.X., Bird, D.K., 2007. High- and ultrahigh pressure metamorphism in the North Qaidam and South Altyn Terranes, western China. International Geology Review 49, 969–995.
Mattinson, C.G., Wooden, J.L., Zhang, J.X., Bird, D.K., 2009. Paragneiss zircon geochronology and trace element geochemistry, North Qaidam HP/UHP terrane, western China. Journal of Asian Earth Sciences 35, 298–309.
Meinhold, G., Reischmann, T., Kostopoulos, D., Frei, D., Larionov, A.N., 2010. Mineral chemical and geochronological constraints on the age and provenance of the eastern Circum-Rhodope Belt low-grade metasedimentary rocks, NE Greece. Sedimentary Geology 229, 207–223.
Meng, Q.-R., Hu, J.-M., Yang, F.-Z., 2001. Timing and magnitude of displacement on the Altyn Tagh fault: constraints from stratigraphic correlation of adjoining Tarim and Qaidam basins, NW China. Terra Nova 13, 86–91.
Menold, C.A., Manning, C.E., Yin, A., Tropper, P., Chen, X.H., Wang, X.F., 2009. Metamorphic evolution, mineral chemistry and thermobarometry of orthogneiss hosting ultrahigh-pressure eclogites in the North Qaidam metamorphic belt, Western China. Journal of Asian Earth Sciences 35, 273–284.
Molnar, P., England, P., Joseph, M., 1993. Mantle dynamics, uplift of the Tibetan plateau and the Indian monsoon. Reviews of Geophysics 31, 357–396.
Morton, A.C., 1985. Heavy minerals in provenance studies. In: Zuffa, G.G. (Ed.), Provenance of Arenites. Reidel, Dordrecht, pp. 249–277.
Morton, A.C., Hallsworth, C.R., 1994. Identifying provenance-specific features of detrital heavy mineral assemblages in sandstones. Sedimentary Geology 90, 241–256.
Morton, A.C., Hallsworth, C.R., 1999. Processes controlling the composition of heavy mineral assemblages in sandstones. Sedimentary Geology 124, 3–29.
Morton, A.C., Hallsworth, C.R., Chalton, B., 2004. Garnet compositions in Scottish and Norwegian basement terrains: a framework for interpretation of North Sea sandstone provenance. Marine and Petroleum Geology 21, 393–410.
Morton, A.C., Whitham, A.G., Fanning, C.M., 2005. Provenance of Late Cretaceous to Paleocene submarine fan sandstones in the Norwegian Sea: integration of heavy mineral, mineral chemical and zircon age data. Sedimentary Geology 182, 3–28.
Morton, A., Hallsworth, C., Strogen, D., Whitham, A., Fanning, M., 2009. Evolution of provenance in the NE Atlantic rift: the Early–Middle Jurassic succession in the Heidrun Field, Halten Terrace, offshore Mid-Norway. Marine and Petroleum Geology 26, 1100–1117.
Morton, A., Ellis, D., Fanning, M., Jolley, D., Whitham, A., 2012. The importance of an integrated approach to provenance studies: a case study from the Paleocene of the Faroe-Shetland Basin, NE Atlantic. Geological Society of America Special Papers 487, 1–12.
Najman, Y., 2006. The detrital record of orogenesis: a review of approaches and techniques used in the Himalayan sedimentary basins. Earth-Science Reviews 74, 1–72.
Rieser, A.B., Neubauer, F., Liu, Y., Ge, X., 2005. Sandstone provenance of north-western sectors of the intracontinental Cenozoic Qaidam basin, western China: tectonic vs. climatic control. Sedimentary Geology 177, 1–18.

Rieser, A.B., Liu, Y., Genser, J., Neubauer, F., Handler, R., Friedl, G., Ge, X.-H., 2006a. $^{40}Ar/^{39}Ar$ ages of detrital white mica constrain the Cenozoic development of the intracontinental Qaidam Basin, China. Geological Society of America Bulletin 118, 1522–1534.

Rieser, A.B., Liu, Y., Genser, J., Neubauer, F., Handler, R., Ge, X.-H., 2006b. Uniform Permian $^{40}Ar/^{39}Ar$ detrital mica ages in the eastern Qaidam Basin (NW China): where is the source? Terra Nova 18, 79–87.

Rieser, A.B., Bojar, A.-V., Neubauer, F., Genser, J., Liu, Y., Ge, X.-H., Friedl, G., 2009. Monitoring Cenozoic climate evolution of northeastern Tibet: stable isotope constraints from the western Qaidam Basin, China. International Journal of Earth Sciences 98, 1063–1075.

Ritts, B.D., Biffi, U., 2001. Mesozoic northeast Qaidam basin: response to contractional reactivation of the Qilian Shan, and implications for the extent of Mesozoic intracontinental deformation in central Asia. Geological Society of America Memoirs 194, 293–316.

Ritts, B.D., Yue, Y., Graham, S.A., Sobel, E.R., Abink, O.A., Stockli, D.F., 2008. From sea level to high elevation in 15 million years: uplift history of the northern Tibetan Plateau margin in the Altun Shan. American Journal of Science 308, 657–678.

Sabeen, H.M., Ramanujam, N., Morton, A.C., 2002. The provenance of garnet: constraints provided by studies of coastal sediments from southern India. Sedimentary Geology 152, 279–287.

Sobel, E.R., Arnaud, N., Jolivet, M., Ritts, B.D., Brunel, M., 2001. Jurassic to Cenozoic exhumation history of the Altyn Tagh range, NW China constrained by $^{40}Ar/^{39}Ar$ and apatite fission track thermochronology. In: Hendrix, M.S., Davis, G.A. (Eds.), Paleozoic and Mesozoic tectonic evolution of central and eastern Asia: from continental assembly to intracontinental deformation: Geological Society of America Memoirs, 194, pp. 1–15.

Song, S.G., Yang, J.S., Xu, Z.Q., Liou, J.G., Wu, C.L., Shi, R.D., 2003a. Metamorphic evolution of coesite-bearing UHP terrane in the North Qaidam, northern Tibet, NW China. Journal of Metamorphic Geology 21, 631–644.

Song, S.G., Yang, J.S., Liou, J.G., Wu, C.L., Shi, R.D., Xu, Z.Q., 2003b. Petrology, Geochemistry and isotopic ages of eclogites in the Dulan UHPM terrane, the North Qaidam, NWChina. Lithos 70, 195–211.

Song, S.G., Zhang, L.F., Niu, Y.L., Su, L., Jian, P., Liu, D.Y., 2005. Geochronology of diamond-bearing zircons from garnet peridotite in the North Qaidam UHPM belt Northern Tibetan Plateau: a record of complex histories from oceanic lithosphere subduction to continental collision. Earth and Planetary Science Letters 234, 99–118.

Song, S.G., Zhang, L.F., Niu, Y.L., Su, L., Song, B., Liu, D.Y., 2006. Evolution from oceanic subduction to continental collision: a case study of the Northern Tibetan Plateau inferred from geochemical and geochronological data. Journal of Petrology 47, 435–455.

Song, S., Su, L., Niu, Y., Zhang, L., Zhang, G., 2007a. Petrological and geochemical constraints on the origin of garnet peridotite in the North Qaidam ultrahigh-pressure metamorphic belt, northwestern China. Lithos 96, 243–265.

Song, S.G., Zhang, L.F., Niu, Y., Wei, C.J., Liou, J.G., Shu, G.M., 2007b. Eclogite and carpholite-bearing metasedimentary rocks in the North Qilian suture zone, NW China: implications for Early Palaeozoic cold oceanic subduction and water transport into mantle. Journal of Metamorphic Geology 25, 547–563.

Song, S., Niu, Y., Zhang, L., Wei, C., Liou, J.G., Su, L., 2009. Tectonic evolution of early Paleozoic HP metamorphic rocks in the North Qilian Mountains, NW China: new perspectives. Journal of Asian Earth Sciences 35, 334–353.

Sun, Z., Yang, Z., Pei, J., Ge, X., Wang, X., Yang, T., Li, W., Yuan, S., 2005. Magnetostratigraphy of Paleogene sediments from northern Qaidam Basin, China: implications for tectonic uplift and block rotation in northern Tibetan plateau. Earth and Planetary Science Letters 237, 635–646.

Takeuchi, M., Kawai, M., Matsuzawa, N., 2008. Detrital garnet and chromian spinel chemistry of Permian clastics in the Renge area, central Japan: implications for the paleogeography of the East Asian continental margin. Sedimentary Geology 212, 25–39.

Tapponnier, P., Xu, Z., Roger, F., Meyer, B., Arnaud, N., Wittlinger, G., Yang, J., 2001. Oblique stepwise rise and growth of the Tibet Plateau. Science 294, 1671–1677.

Tolosana-Delgado, R., 2012. Use and misuse of compositional data in sedimentology. Sedimentary Geology 280, 60–79.

von Eynatten, H., Gaupp, R., 1999. Provenance of Cretaceous synorogenic sandstones in the Eastern Alps: constraints from framework petrography, heavy mineral analysis and mineral chemistry. Sedimentary Geology 124, 81–111.

Wang, J., Wang, J.Y., Liu, Z.C., Li, J.Q., Xi, P., 1999. Cenozoic environmental evolution of the Qaidam Basin and its implications for the uplift of the Tibetan Plateau and the drying of central Asia. Palaeogeography, Palaeoclimatology, Palaeoecology 152, 37–47.

Wang, E., Xu, F.-Y., Zhou, J.-X., Wan, J., Burchfiel, B.C., 2006. Eastward migration of the Qaidam basin and its implications for Cenozoic evolution of the Altyn Tagh fault and associated river systems. Geological Society of America Bulletin 118, 349–365.

Wang, X., Qiu, Z., Li, Q., Wang, B., Qiu, Z., Downs, W.R., Xie, G., Xie, J., Deng, T., Takeuchi, G.T., Tseng, Z.J., Chang, M., Liu, J., Wang, Y., Biasatti, D., Sun, Z., Fang, X., Meng, Q., 2007. Vertebrate paleontology, biostratigraphy, geochronology, and paleoenvironment of Qaidam Basin in northern Tibetan Plateau. Palaeogeography, Palaeoclimatology, Palaeoecology 254, 363–385.

Wang, Q., Pan, Y., Chen, N., Li, X., Chen, H., 2009. Proterozoic polymetamorphism in the Quanji Block, northwestern China: evidence from microtextures, garnet compositions and monazite CHIME ages. Journal of Asian Earth Sciences 34, 686–698.

Weltje, G.J., 2002. Quantitative analysis of detrital modes: statistically rigorous confidence region in ternary diagrams and their use in sedimentary petrology. Earth-Science Reviews 57, 211–253.

Weltje, G.J., 2006. Ternary sandstone composition and provenance: an evaluation of the "Dickinson model". In: Buccianti, A., Mateu-Figueras, G., Pawlowsky-Gahn, V. (Eds.), Compositional Data Analysis in the Geosciences: From Theory to Practice: Geological Society of London. Special Publications, London (79-99 pp.).

Weltje, G.J., 2012. Quantitative models of sediment generation and provenance: state of the art and future developments. Sedimentary Geology 280, 4–20.

Weltje, G.J., von Eynatten, H., 2004. Quantitative provenance analysis of sediments: review and outlook. Sedimentary Geology 171, 1–11.

Win, K.S., Takeuchi, M., Tokiwa, T., 2007. Changes in detrital garnet assemblages related to transpressive uplifting associated with strike–slip faulting: an example from the Cretaceous System in Kii Peninsula, Southwest Japan. Sedimentary Geology 201, 412–431.

Yang, J.S., Wu, C.L., Zhang, J.X., Shi, R.D., Meng, F.C., Wooden, J., Yang, H.Y., 2006. Protolith of eclogites in the north Qaidam and Altun UHP terrane NW China: earlier oceanic crust? Journal of Asian Earth Sciences 28, 185–204.

Yavuz, F., Gultekin, A.H., Karakaya, M.C., 2002. CLASTOUR: a computer program for classification of the minerals of the tourmaline group. Computer Geoscience 25, 1017–1036.

Ye, D., Zhong, X., Yao, Y., Yang, F., Zhang, S., Jiang, Z., Wang, Y., 1993. Tertiary Strata in Chinese Petroliferous Provinces (volume I) — the General. Petroleum Industry Press, Beijing, China (156-159 pp. (in Chinese)).

Yin, A., Rumelhart, P.E., Butler, R.E., Cowgill, E., Harrison, T.M., Foster, D.A., Ingersoll, R.V., Zhang, Q., Zhou, X.-Q., Wang, X.-F., Hanson, A., Raza, A., 2002. Tectonic history of the Altyn Tagh fault system in northern Tibet inferred from Cenozoic sedimentation. Geological Society of America Bulletin 114, 1257–1295.

Yu, S., Zhang, J., Li, J., Meng, F., 2010. Zircon U–Pb geochronology of high-pressure granulite and its tectonic implications in the Dulan area, North Qaidam Mountains, western China. Acta Petrology Et mineralogy 29, 139–150 (In Chinese with English abstract).

Yue, Y., Ritts, B.D., Graham, S.A., Wooden, J.L., Gehrels, G.E., Zhang, Z., 2003. Slowing extrusion tectonics: lowered estimate of post-Early Miocene slip rate for the Altyn Tagh fault. Earth and Planetary Science Letters 217, 111–122.

Zhang, J., Zhang, Z., Xu, Z., Yang, J., Cui, J., 2000. Discovery of khondalite series from the western segment of Altyn Tagh and their petrological and geochronological studies. Science in China Series D: Earth Sciences 43, 308–316.

Zhang, J., Zhang, Z., Xu, Z., Yang, J., Cui, J., 2001. Petrology and geochronology of eclogites from the western segment of the Altyn Tagh, northwestern China. Lithos 56, 187–206.

Zhang, J., Meng, F., Yang, J., 2004. Eclogitic metapelites in the western segment of the north Qaidam Mountains: evidence on "in situ" relationship between eclogite and its country rock. Science in China Series D: Earth Sciences 47, 1102–1112.

Zhang, J.X., Yang, J.S., Mattinson, C.G., Xu, Z.Q., Meng, F.C., Shi, R.D., 2005. Two contrasting eclogite cooling histories, North Qaidam HP/UHP terrane, western China: petrological and isotopic constraints. Lithos 84, 51–76.

Zhang, J., Meng, F., Yu, S., Qi, X., 2007. Metamorphic history recorded in high pressure mafic granulites in the Luliangshan Mountains to the north of Qaidam Basin, northwest China: evidence from petrology and zircon SHRIMP geochronology. Earth Science Frontiers 14, 85–97 (In Chinese with English abstract).

Zhang, G., Song, S., Zhang, L., Niu, Y., 2008a. The subducted oceanic crust within continental-type UHP metamorphic belt in the North Qaidam, NW China: evidence from petrology, geochemistry and geochronology. Lithos 104, 99–118.

Zhang, J., Mattinson, C.G., Meng, F., Wan, Y., Tung, K., 2008b. Polyphase tectonothermal history recorded in granulitized gneisses from the north Qaidam HP/UHP metamorphic terrane, western China: evidence from zircon U–Pb geochronology. Geological Society of America Bulletin 120, 732–749.

Zhang, G., Zhang, L., Song, S., Niu, Y., 2009a. UHP metamorphic evolution and SHRIMP geochronology of a coesite-bearing meta-ophiolitic gabbro in the North Qaidam, NW China. Journal of Asian Earth Sciences 35, 310–322.

Zhang, J.-X., Mattinson, C.G., Meng, F.-C., Yang, H.-J., Wan, Y.-S., 2009b. U–Pb geochronology of paragneisses and metabasite in the Xitieshan area, north Qaidam Mountains, western China: constraints on the exhumation of HP/UHP metamorphic rocks. Journal of Asian Earth Sciences 35, 245–258.

Zhang, L., Wang, Q., Song, S., 2009c. Lawsonite blueschist in Northern Qilian, NW China: P–T pseudosections and petrologic implications. Journal of Asian Earth Sciences 35, 354–366.

Zhuang, G., Hourigan, J.K., Ritts, B.D., Kent-Corson, M.L., 2011. Cenozoic multiple-phase tectonic evolution of the northern Tibetan Plateau: constraints from sedimentary records from Qaidam basin, Hexi Corridor, and Subei basin, northwest China. American Journal of Science 311, 116–152.

Zuffa, G.G., 1985. Optical analyses of arenites: influence of methodology on compositional results. In: Zuffa, G.G. (Ed.), Provenance of Arenites, NATO Advanced Study Institute, vol. 148. D. Reidel, Dordrecht, pp. 165–189.